Evaluation of Optical Losses in Silicon Waveguide Spot-size Converters

A THESIS

submitted by

MEENATCHI SUNDARAM S

for the award of the degree

of

MASTER OF SCIENCE

(by Research)

DEPARTMENT OF ELECTRICAL ENGINEERING.
INDIAN INSTITUTE OF TECHNOLOGY MADRAS.

Dec 2018

CERTIFICATE

This is to certify that the thesis titled **Evaluation of Optical Losses in Silicon Waveguide Spot-size Converters**, submitted by **Meenatchi Sundaram S**, to the Indian Institute of Technology, Madras, for the award of the degree of **Master of Science**, is a bona fide record of the research work done by him under my supervision. The contents of this thesis, in full or in parts, have not been submitted to any other Institute or University for the award of any degree or diploma.

Prof. Bijoy Krishna Das
Research Guide
Dept. of Electrical Engineering
IIT-Madras, PIN - 600 036

Place: Chennai, India

Date: Sat 12th Jan, 2019

Make Hay While the Sun Shines

ACKNOWLEDGEMENTS

I am indebted to Prof. Bijoy Krishna Das for his diligent guidance and patience through out my research work. His guidance has been positively sculpturing my research career as well as personal life. I wish to thank my General Test Committee (GTC) Dr. Anant Krishnan and Prof. Prem B. Bisht for their valuable advice and suggestions. I would like to thank the faculties of Center for NEMS and Nanophotonics (CNNP), who are instrumental in maintaining the laboratory condition in greater standard . I would like to thank Prof.Vijayan C for his course on Non linear optics, which kindled lot of interest towards the subject. I would like to thank my teachers Prof. Anjan chakraborthy, Prof. Kalmarkar, Prof Balaji Srinivasan and Prof. Deepa venkitesh for laying the foundation for my research through their teaching.

The Integrated Optoelectronics group at IIT Madras has always been accommodative and I am fortunate enough to be associated with the group. I specially thank Mr Sakthivel and Dr Sujith for their help in various stages of my research and to get a hands-on in fabrication, optical characterization. I thank all my friends Mr. Saket, Ms. Riddhi, Ms. Sumi, Mr. Vivek, Dr. Shantanu, Mr. Harish, Mr. Gaurang, Mr. Narendran, Mr.Solomon, Mr. Ramesh, Dr. Parimal, Mr. Rajat, Mr. Deepak, Ms. Rashmi, Ms. Sireesha, Mr. Sreevatsa, Dr. Srivatsa, Mr. Chaitanya, Mr. Uppu Karthik, Mr. Dadavali, Dr. John and Mr. Rupesh for their moral support, active participation during group meetings and paving a successful way for silicon photonics research at IIT Madras. I thank Mr. Rajendran, Mr. Prakash, Mr. Venkatesh, Mr. Joseph for their support during waveguide fabrication.

I thank Dr. Vijayakumar, Mr. Vinoth, Ms. Gayathri, Mr. Bhadri, Dr. Aneesh Bekal, Mr.Prashanth David and Dr. Aravind for their external help in various occasions. I thank, the Lord almighty for teaching me valuable experiences through this opportunity. Last but not the least I would like to thank my parents, sister, my wife and my son for their unconditional love, patience and support.

ABSTRACT

KEYWORDS: Silicon Photonics, Optical interconnect, Tapered waveguides, Spot-size converters, Sidewall roughness, Scattering loss

The evolution of CMOS compatible silicon photonics technology enabled high speed on-chip optical interconnects, accurate label-free bio-sensing and finding various futuristic novel applications. Commercial availability of optical grade silicon-on-insulator wafers has helped to realize low-loss photonic wire waveguide devices (active/passive) leading towards the demonstrations of application specific photonics circuits with large-scale integration. The waveguide spot-size converters (SSC) are essentially used at the input/output of an integrated silicon photonics chip for fiber-optic interfacing and on-chip impedance/mode matching between waveguide components. Typical length of a silicon photonic waveguide SSC can vary from a few micrometers to several millimeters depending on device geometry and applications. Therefore, the propagation loss in SSC can be significant and it can be minimized by optimizing design parameters. The existing models available for calculating the propagation loss (mainly scattering loss due to surface roughness) is limited to straight waveguide in the literature and there is no model available for estimating the scattering loss in the SSC. In the present work, we propose a generalized scattering loss model for SSC by extending the straight waveguide scattering model, incorporating the influential parameters for SSC design such as geometry for single mode condition, shape of the cross section, suitable SSC profile and experimental parameters like roughness, correlation length. The proposed model has been validated with experimental results obtained from the devices fabricated indigenously and reported elsewhere in literature.

TABLE OF CONTENTS

LIST OF TABLES

LIST OF FIGURES

ABBREVIATIONS

Acronyms

C-Band	Conventional wavelength band ($\lambda \sim 1527$ to 1567 nm)
L-Band	Long wavelength band ($\lambda \sim 1567$ to 1607 nm)
WDM	Wavelength-division-multiplexing
SSC	Spot-size Converter
CMOS	Complementary Metal Oxide Semiconductor
DI	De-ionized (water)
DUT	Device Under Test
EDFA	Erbium Doped Fiber Amplifier
FCA	Free Carrier Absorption
FSR	Free Spectral Range
ICP	Inductively Coupled Plasma
IL	Insertion Loss
MZI	Mach Zehnder Interferometer
PDL	Polarization Dependent Loss
PPR	Positive Photo Resist
RIE	Reactive Ion Etching
SEM	Scanning Electron Microscope
SMF	Single Mode Fiber
SOI	Silicon-On-Insulator
TE	Transverse Electric (polarization)
TM	Transverse Magnetic (polarization)
TPA	Two Photon Absorption
UV	Ultra-Violet

Chemical Names

Al	Aluminum

Ar	Argon
Cr	Chromium
HCl	Hydrochloric Acid
HF	Hydrofluoric Acid
HNO_3	Nitric Acid
H_2O	Water
H_2O_2	Hydrogen Peroxide
H_2SO_4	Sulphuric Acid
SF_6	Sulfur Hexafluoride
Si	Silicon
SiO_2	Silicon dioxide
TCE	Tri-chloro Ethylene
TMAH	Tetramethylammonium Hydroxide

Units

dB	decibel
dBm	decibel milli-watt
mW	milli watt
µW	micro watt
µm	micrometer
ns	nano Second
µs	micro second
sccm	standard cubic centimeter per minute
mTorr	milli-Torr (of pressure)
mbar	milli-Bar (of pressure)
ml	milli-liter (of fluid)

NOTATION

$\mathbf{n}$	Refractive index
$\mathbf{n}_{eff}$	Effective refractive index
$\boldsymbol{\epsilon}$	Permitivity
$\boldsymbol{\lambda}$	Wavelength
$\boldsymbol{\beta}$	Propagation constant
$\boldsymbol{\beta_{TPA}}$	Two Photon Absorption coefficient
$\boldsymbol{\phi}$	Phase of the EM wave
$\mathbf{L}$	Length
$\boldsymbol{\alpha}$	Loss per unit length

CHAPTER 1

Introduction

Waveguide Spot-Size Converters (SSCs) play a vital role in integrated silicon photonics chip for input/output light coupling [1, 2] and on-chip mode matching/conversion [3, 4]. In this chapter, a general introduction about optical interconnects, state of the art SSC structures used for on-chip and off-chip applications, the origination of roughness in a straight waveguide and related propagation loss, followed by research objective of this work have been discussed.

1.1 Motivation

Silicon photonics has been looked upon for versatile applications ranges from high speed optical interconnects, switching, quantum computing to accurate bio-sensing elements [5, 6, 7]. This is due to the feasibility of confining light into different cross sections and the use of adaptable CMOS fabrication process for making the waveguides. The growing need for compact devices made a drive towards nano dimensioned, compact silicon photonic components. Low loss, smaller cross section silicon waveguides and its processing has been looked towards the development of system-on-chip applications and sensors. A pioneer in Si photonics R A soref [8], has proposed a "super chip" in which photonic and electronic processing circuits can co-exist on a Si chip in different layers as shown in Figure 1.1. The bottom layer in the Figure 1.1, is an electronic processing part and in the top layer, photonic functional circuits have been placed. The proposed integration helps in faster data transfer using photonic devices and process the data via electronic devices which results in manifold increment in speed of data processing. Such a monolithic integration of electronic and photonic components has reduced power/bit and cost. A similar technique exist for making the optical interconnects based on waveguides, on silicon nitride, Gallium Arsenide (GaAs), Glass and Indium Phosphide (InP) etc., and other material platforms. The refractive index

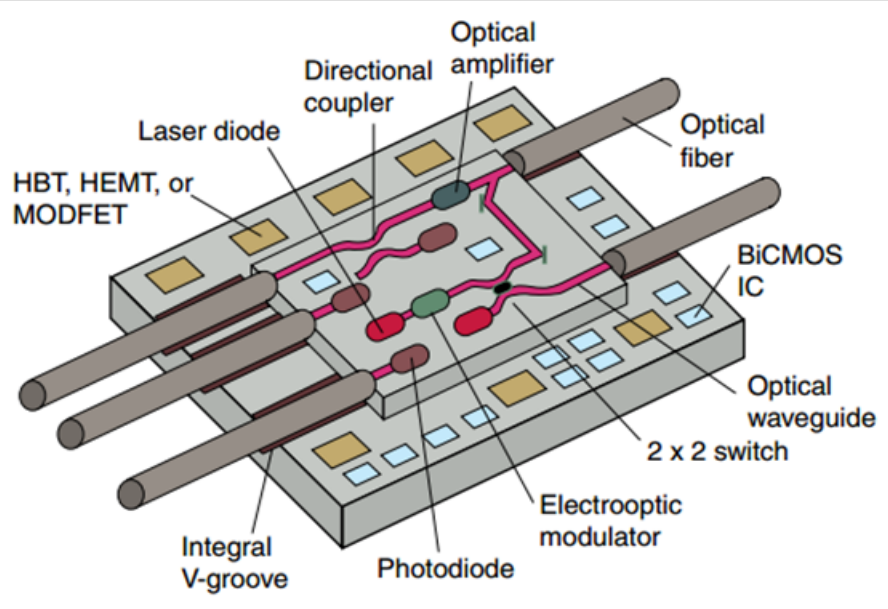

Figure 1.1: Scheme of a "super chip" in silicon platform by R A Soref on 1993 [8]

contrast between BOX (lower cladding) and device layer silicon in SOI allows to fabricate compact photonic wire devices. But coupling light from optical fiber to photonic wire waveguide dimension lead to large mode mismatch loss. The mode profiles of a standard single mode, optical fiber (SMF) having $\sim$ 10 μm radius and a photonic wire waveguide (W- 500 nm, H- 220 nm) at wavelength λ =1550 nm, are shown in figure 1.2 to visualize the mode size difference. The large mode mismatch results in poor coupling efficiency as low as 0.1% between single mode fiber having radius $\sim$ 9 μm and a photonic wire waveguide 220 nm x 450 nm [9].

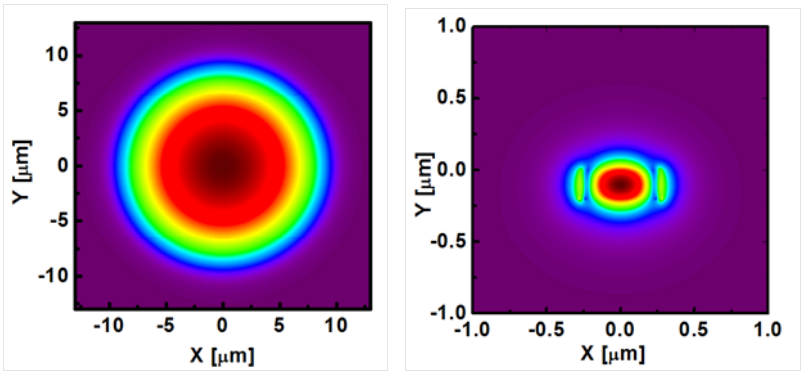

(a) (b)

Figure 1.2: (a) Comparison of mode profiles of standard SMF - 10 μm radius; (b) Photonic wire waveguide (W - 500 nm, H- 220 nm).

SSCs have been the option for interfacing the smaller waveguide cross section to

larger waveguide cross section. SSCs are tapered waveguides which change the dimensions of input and output side of the cross section gradually to improve coupling loss, enhance optical modulation and etc., The classical approach for SSCs fabrication is to make an inverse tapering structure as shown in Figure 1.3 with the suitable cladding material for a particular length. The inverse taper structure has small waveguide width

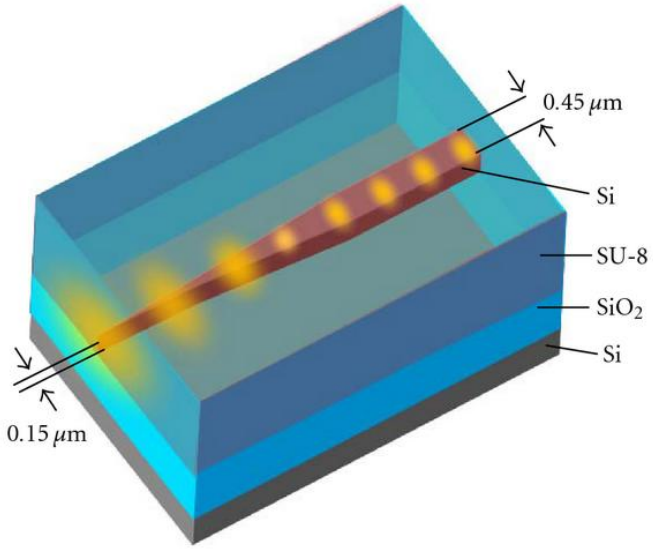

Figure 1.3: Schematic representation of a guided mode spot-size conversion in a inverse tapered SSC [10].

($\sim$ 0.12 μm - 0.15 μm) in the input side and gradually expanded along propagation direction to a desired photonic wire waveguide dimension ($\sim$ 0.4 μm -0.5 μm) with a suitable cladding. Near the input, since the dimensions of the waveguide core is small, the mode is expanded into the top cladding which matches with the fiber mode to reduce the mode mismatch. Besides, due to the mode expansion, the effective index of the mode reduces and matches with the fiber core effective index. This effective index matching reduces Fresnel reflection loss since the light is launched from optical fiber core (n $\sim$ 1.45) to silicon photonic wire waveguide (n $\sim$ 3.45)). In all these cases, SSCs have been employed to reduce the coupling loss and enhancing the integration of functional devices. The total insertion loss of SSC consists of mode mismatch loss, Fresnel reflection loss and scattering loss. The scattering loss in SSC converter is a major component as the length of SSC varies from μms to several millimeters.

1.2 State of the art SSC structures

SSCs have been fabricated using many techniques to reduce the coupling loss, improve the mode field enhancement with the material and etc., In one case [1], the width of waveguide in the input side is kept at 120 nm and is gradually expanded to the final width of 450 nm through a parabolic taper structure [1] as shown in Figure 1.4(a). The tip was kept slightly offset from the edge to further allow the mode expansion. The mode is expanded to match fiber mode profile to reduce the coupling loss. It is to be noted that fabricating high aspect ratio structures (H/W - 220 nm / 120 nm) at the input side is technologically challenging. The reported insertion loss for this structure was $\sim$ 6 dB for 40 μm length.

By referring to Figure 1.4(b) in [11], the designed structure consist of both forward and inverse taper together to engineer the effective index of the tapered section to couple the light from fiber to photonic wire waveguide. The corresponding mode size reduction has also been shown in the figure1.4(b). The input side of this structure has been made of low index waveguide which results in low coupling loss of $\sim$ 0.6 dB.

Various fabrication techniques have been explored [12, 13, 14, 15, 16] to modify the cross section of a waveguide. Recently a novel post-fabrication method for monolithic integration of higher and small cross section waveguides has been proposed in [17].

A new technique for reducing the polarization dependencies have been in reported in [18]. A knife edge structure as shown in Figure 1.5 has a gradual height reduction (from 220 nm to 110 nm) apart from existing width reduction, at the edge which helps in reducing mode conversion loss by making an adiabatic transition at the tip. The light input is given from the edge, so that fiber mode matches with waveguide mode.

Figure 1.6 shows a photonic wire waveguide has been connected to a higher dimensioned SSC, adjacent to a grating coupler [2]. Although grating couplers are used for coupling light in and out of the waveguide, they require a larger coupling area to match the fiber dimension. This is an example for on-chip integration of two functional components such as a grating coupler and a photonic wire waveguide through a SSC. The estimated coupling efficiency in the structure was 97 % but post the fabrication it

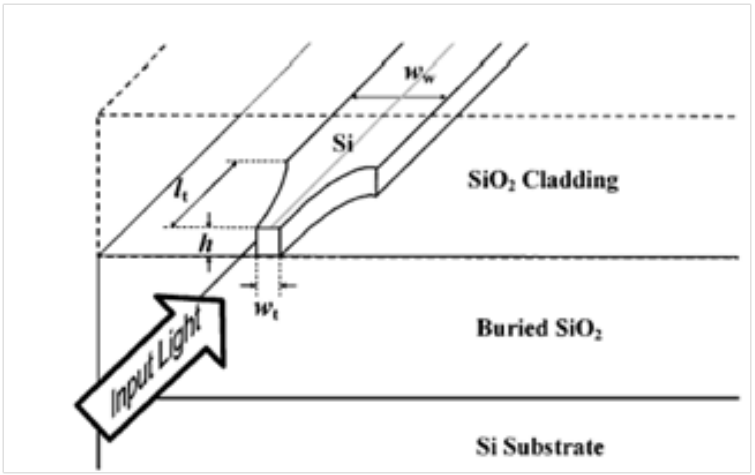

(a)

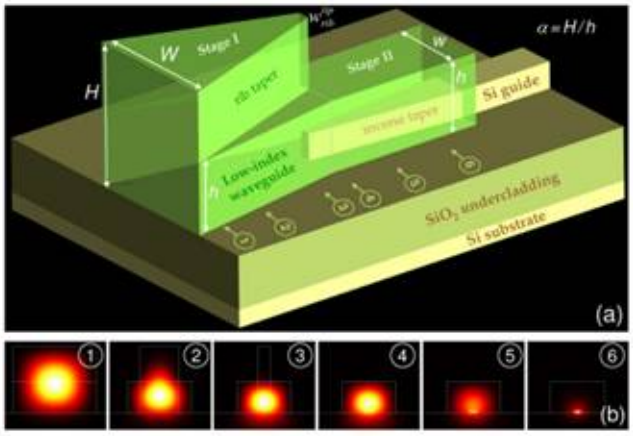

(b)

Figure 1.4: (a) A SSC based on inverse taper having parabolic variation from input [1] ; (b) Effective index engineering in SSC using the combination of forward and inverse taper [11].

reduced to 47 %, mainly due to scattering at the grating region.

Forward taper based SSC has initially higher cross section and tapered down to the desired waveguide dimension with a suitable SSC profile. Since the dimension is higher in the input side, the effective index is higher which may not match with the fiber mode effective index which leads to unavoidable Fresnel loss in the facet of the waveguide.

Apart from coupling light into the waveguide, there is also challenge in integrating many functional devices having different device layer thicknesses. For example, a GeSi based electroabsorption modulator [19] has been integrated with silicon based SSC as shown in Figure 1.7. This modulator works best on smaller cross section on silicon-germanium platform as Franz-Keldysh effect is high and lower electric field is required

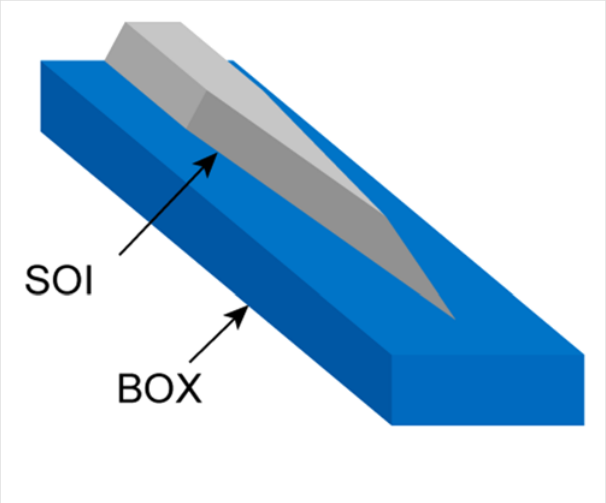

Figure 1.5: Schematic of knife edge inverse taper based SSC [18].

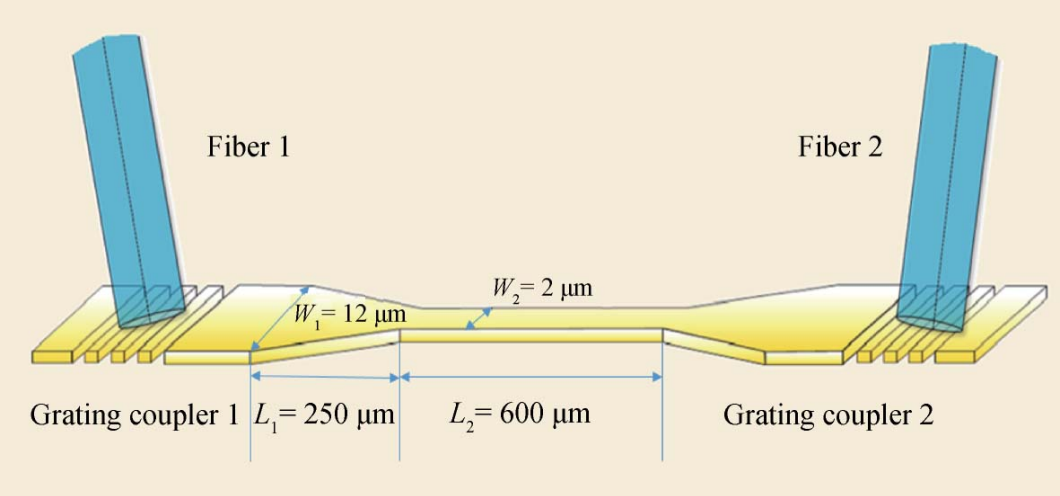

Figure 1.6: Grating coupler integrated with forward taper based SSC [2].

for realizing the modulation.

The summary of on-chip and off-chip applications of SSC is listed in the Table 1.1. It shows the loss of SSC varies from 0.5 dB to 4.5 dB for varying lengths (from 40 μm to 1 mm). The exposure of mode to longer length (more exposure to roughness) will increase the scattering loss and shorter length may result in non-adiabatic propagation. It is understandable that an optimum length has to be decided by choosing adiabatic SSC profile with considerably less exposure to roughness.

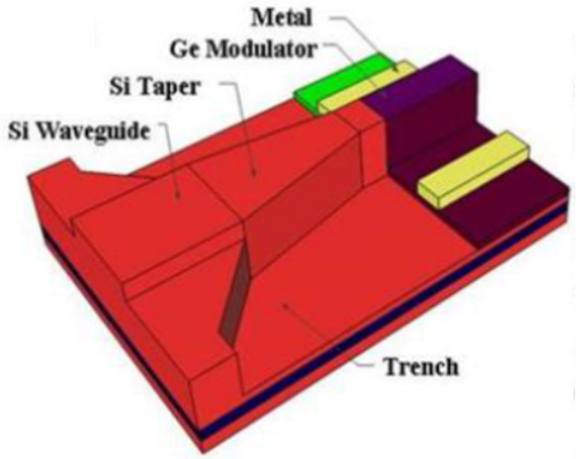

Figure 1.7: Spot-size converter used in SOI platform to integrate Ge electroabsorption modulator [19].

Table 1.1: SSC types and losses

Application	**SSC Type**	**SSC Length**	**SSC Loss**
Off-chip coupling	Inverse taper [1]	40 μm	4.5 dB
Off-chip coupling	Inverse taper [11]	256 μm	0.6 dB
Off-chip Coupling	Forward taper with Grating coupler [2]	250 μm	3.2 dB
On-chip Coupling	Forward taper integrating two cross sections[20]	1 mm	0.5 dB

1.2.1 Scattering loss induced from fabrication process

The roughness originates from photolithography process during the fabrication of silicon waveguides which is called pattern induced roughness. The induced roughness is further aggravated by Reactive Ion Etching (RIE) process step. Figure 1.8 shows roughness in the sidewall of a straight Si waveguide.

The presence of roughness in the SSC structure leads to scattering loss. The loss estimation methods reported till now mostly aimed at modeling the scattering loss in photonic wire dimensions. The modeling of roughness induced scattering loss in straight waveguides has been explored for decades, right from Payne and Lacey [22] . Accurate modeling of straight waveguide loss by Magnetic Resonance Imaging (MRI) ex-

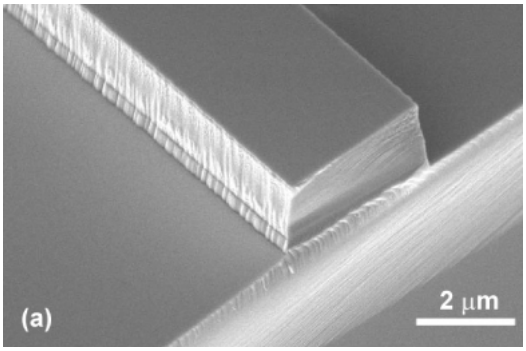

Figure 1.8: Fabricated Si waveguide showing roughness in the sidewall [21]

perimental waveguide data and solving modal equations has been discussed [23]. Loss modeling of an inverse tapering using effective index variation because of width change has been explained. Though the model accounts for the roughness in the photonic wire nano taper, it does not explicitly talk about fabrication induced roughness in the top surface and modeling of a non-ideal cross sections arises out of fabrication procedure followed. Moreover, the total taper loss includes considerable amount of mode conversion loss because of non-adiabatic nature of the structure i.e., if the designed dimension falls under multimode in the SSC propagation region, it may lead to additional mode conversion loss.

1.3 Research Objective

It is necessary to quantify the scattering loss that is induced by the roughness since methods are available to estimate mode mismatch loss and Fresnel loss in a SSC. There are scattering loss model available for estimating the propagation loss in straight waveguides and there is no model available to account roughness induced scattering loss in a SSC as the length of structure varying (ranges from ~ 40 μm to 1 mm) leading to considerable amount of interaction between roughness and the propagating mode. A generalized scattering loss modeling for any defined SSC length, adiabatic/non-adiabatic tapered SSC waveguide with any cross section, roughness in the sidewalls/surface has not been explored for evaluating the scattering loss which is the objective of this work.

1.4 Thesis Organization

The chapters of this thesis are organized as follows: In the first chapter, an introduction about Silicon photonics and its development, application have been discussed. The chapter also explains about the state of the art SSC structures available, application and roughness effect on this structures. Then the bottlenecks in packaging the Si photonic devices have been discussed, followed by, research objective has been defined for loss estimation in SSC silicon waveguides, the need and application for such model has been explained.

In the second chapter, a numerical model for estimating scattering loss in the SSC has been proposed with the help of forward and inverse taper based SSC have been explained. The parameters influencing the loss such as single mode condition, SSC length, slope of the taper, RMS roughness, correlation length have been discussed.

In the third chapter, the proposed model has been validated with the fabricated and reported SSC. The fabrication process flow of the forward taper based SSC considered for validation, has been discussed. The methodology followed for validation of the model has been discussed.

In the fourth chapter, the results obtained from modeling and validation has been summarized and application of the model for calculating nonlinear losses has been discussed.

CHAPTER 2

Scattering loss in SSC: Theoretical Modeling

In this chapter, the roughness induced scattering losses have been discussed for one dimensional and two dimensional SSC. A new model has been proposed for estimating the scattering loss in SSC. The influential parameters on scattering loss such as RMS roughness, correlation length, length of the SSC, shape of the cross section, single mode condition in the waveguide for the defined dimensions, profile of variation have been considered for the analysis to understand the underlying losses comprehensively. The attempted model has been generalized to work for any defined dimensions of the waveguide and SSC profile.

2.1 Scattering loss in an one dimensional waveguide

The propagation of light in the waveguide is aided by refractive index contrast and total internal reflection. As the Figure 2.1 shows, one dimensional waveguide refers to refractive index variation in one axis. The structure in left in figure 2.1, is a hypothetical structure, is infinitely long in Z direction and has refractive index variation in Y-axis. The interface between core and cladding is the region where roughness predominantly induces the scattering loss. Due to the continuity of tangential component of electric field at the boundary, these roughness act as an antenna and radiate away the energy. If the magnitude of electric field is higher near the interface, then the interaction with the roughness is higher, so is the scattering induced radiation loss.

The scattering loss for one dimensional waveguide is given by Payne-Lacey model, by which the loss is mainly influenced by RMS value of roughness, correlation length, effective index and intensity of the light at interface of the waveguide.

The roughness variation, as seen in Figure 2.1 (left) is statistical and is thought to be superposition of many spatial frequencies. The identification of the major component of

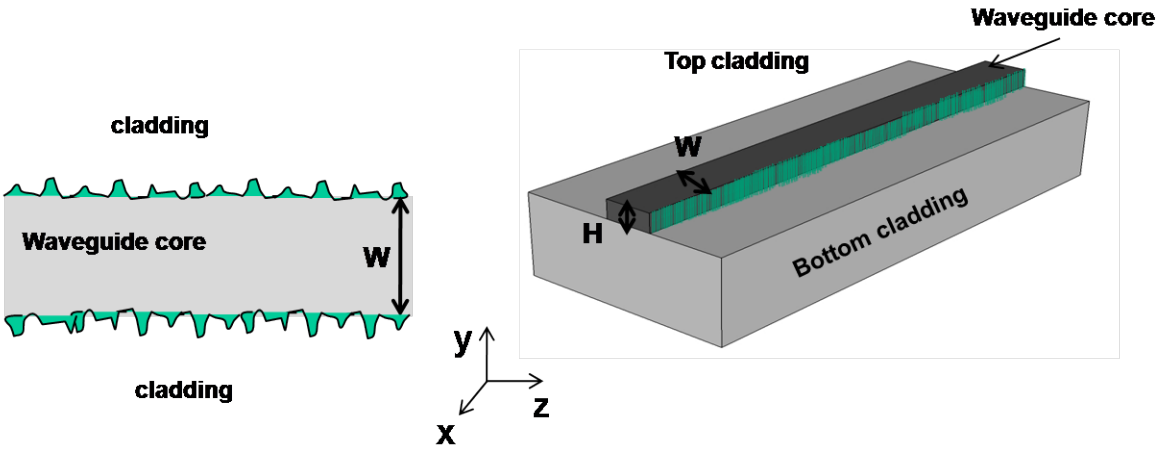

Figure 2.1: Schematic representation of typical 1D and SOI based 2D optical waveguides along with side-wall roughness because of lithographic limitations.

the frequency present in the roughness profile and taking the inverse Fourier transform lead to the choosing the right value of auto correlation length. Both the roughness and autocorrelation length are experimental parameters as a result of etching process.

At correlation length (L_c), the roughness value reduces to (1/e) its initial value. The scattering loss in such a one dimensional waveguide is given below,

$$\alpha = (\frac{\sigma^2}{k_0\sqrt{2}d^4 n_c})gf \tag{2.1}$$

$$g = \frac{U^2V^2}{W} \tag{2.2}$$

$$U = k_0 d\sqrt{(n_c^2 - n_{eff}^2)} \tag{2.3}$$

$$V = k_0 d\sqrt{(n_c^2 - n_{cl}^2)} \tag{2.4}$$

$$W = k_0 d\sqrt{(n_{eff}^2 - n_{cl}^2)} \tag{2.5}$$

$$f = \frac{x\sqrt{1 - x^2 + \sqrt{(1+x^2)^2 + 2X^2\gamma^2}}}{\sqrt{(1+x^2)^2 + 2X^2\gamma^2}} \tag{2.6}$$

$$x = \frac{WL_c}{d}, \gamma = \frac{n_c V}{\sqrt{\Delta}} \tag{2.7}$$

Here, σ is RMS value of roughness

d - Half width of waveguide

k_0 - Propagation constant of wave in free space

n_c - Core refractive index

n_{cl} -Cladding refractive index

L_c - Correlation length

The equations above can be used to study loss in a 1D waveguide structure.

2.2 Loss estimation of SSCs with 1D Tapering

Two dimensional waveguides refer to refractive index variation in X and Y axis of the waveguide. This structure has a finite length in Z direction. The strip waveguide in Figure 2.1 (right) has two dimensional refractive index contrast that allows mode confinement in two axes. These are realizable waveguide structures where Payne and Lacey model can be directly applied with the help of effective index method. The propagation loss in the waveguide can also be measured experimentally using Cut back method or Fabry-Perot measurement method.

An inverse taper based 1D SSC has been used to explain the proposed model. The scheme of the inverse taper based SSC has been shown in Figure 2.2 . The width in the structure varies from 120 nm to 400 nm for a length of 40 μm. Since only width is changed to design a SSC, this is called as 1D SSC. It is worth mentioning here that for a waveguide to guide, it requires 2D refractive index contrast and to denote the structural variation in SSC, 1D notation has been used. The dimensions mentioned are chosen based on the literature [1], except the profile of SSC. A linear profile variation has been considered for simplicity. The height of the device (Thickness of device layer in SOI wafer) is 220 nm. The cross section used in the structure is shown in Figure 2.3. As can seen, it has a lower dimension initially to allow mode expansion, and increased to the functional waveguide dimension along the propagation length. The width variation is defined by the slope equation below,

$$W(z) = W_0 + mL \tag{2.8}$$

where, m-slope of the variation L- SSC length

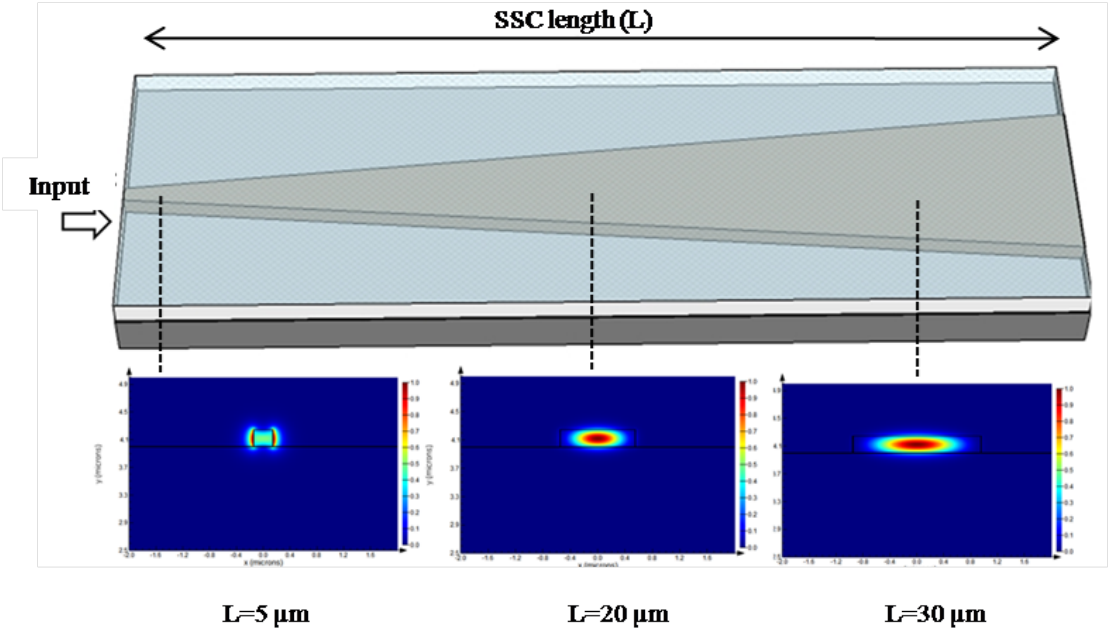

Figure 2.2: Scheme of 1D SSC with mode profiles along the SSC length.

The cross section considered in Figure 2.3 is an ideal cross section with the perpendicular sidewall in the waveguide.

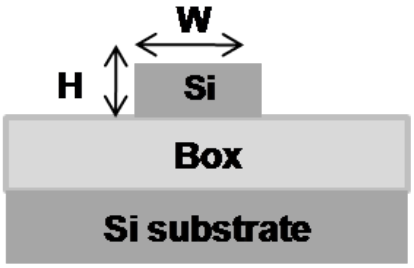

Figure 2.3: Scheme of the cross section used in 1D SSC.

The loss in such a structure is generally a function of variations in device layer thickness and width along SSC propagation length. The structure can be thought as continuously varying cross sections that are stacked together. Mode profiles along SSC length has been shown in Figure 2.2. The loss in this structure would be varying because of dimensional change, through out the propagation length which we define as distributed loss. The distributed loss including its influential parameters is given below,

$$\alpha_d(z) = A(S_w(z) + S_H(z) + S_h(z)) \tag{2.9}$$

$$S_w(Z) = \frac{dn_{eff}}{dW}(Z) \tag{2.10}$$

$$S_H(Z) = \frac{dn_{eff}}{dH}(Z) \tag{2.11}$$

$$S_h(Z) = \frac{dn_{eff}}{dh}(Z) \tag{2.12}$$

$$\tag{2.13}$$

As there is no height and slab height variations in the considered structure, the equation modifies to,

$$\alpha_d(z) = AS_w(z) \tag{2.14}$$

The value S_W denotes of the variation of effective index of SSC taper due to variation of width. The term A relates to roughness and correlation length [24].

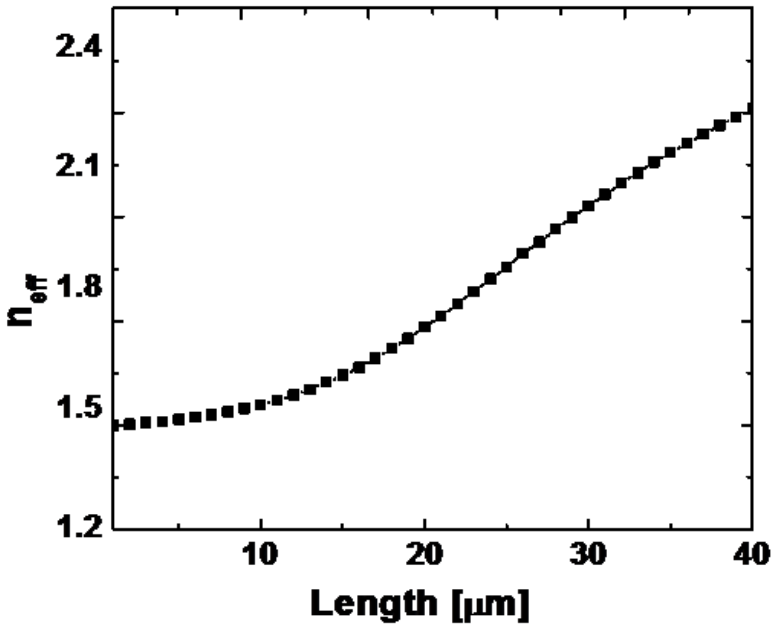

Figure 2.4: Calculated effective index as a function of SSC length.

The figure 2.4 shows the effective index (TE_0 fundamental mode) variation due to cross sectional change. The value of dn_{eff}/dW has been calculated changing the width of tapered SSC to 0.02 μm (dW) at every point of its length and calculating the effective index change as shown in Figure 2.5. The loss is dependent on roughness and correlation length and these two are decided by the fabrication process recipe. The

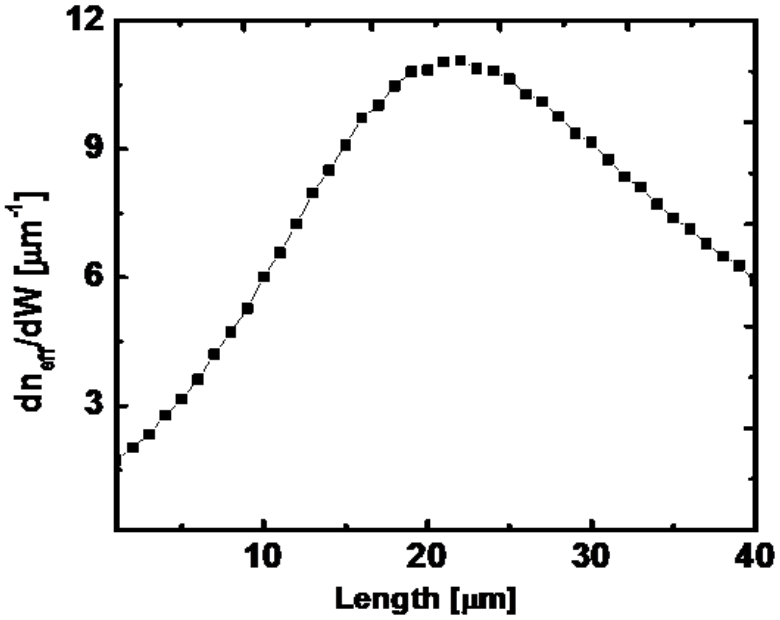

Figure 2.5: Calculated $\frac{dn_{eff}}{dW}$ as a function of length for a SSC length of 40 μm, input width 120 nm, output width 400 nm and device layer thickness 220 nm.

total loss can be calculated by integrating the distributed loss over the SSC length as depicted in equation 2.16. The RMS roughness value was taken to be 20 nm and the correlation length was taken from the literature 50 nm [24]. The justification for the value of roughness comes from the range of roughness values achievable in the CMOS process flow (5 nm - 25 nm) while fabricating a waveguide. The total insertion loss for this structure has been estimated to be $\sim$ 3.5 dB/SSC. The dn_{eff}/dW have been substituted in equation 9 and distributed loss in the SSC has been calculated.

$$\alpha_T = \int \alpha_d(L)\, dL \tag{2.15}$$

2.3 Loss estimation of SSCs with 2D tapering

A rib waveguide based 2D SSC has been considered for calculation .The cross section considered for effective index calculation has been shown in Figure 2.8. In this special case where all the height, slab height and width of a rib waveguide is reduced simultaneously along propagation length. Since all, height, slab height and width are reduced

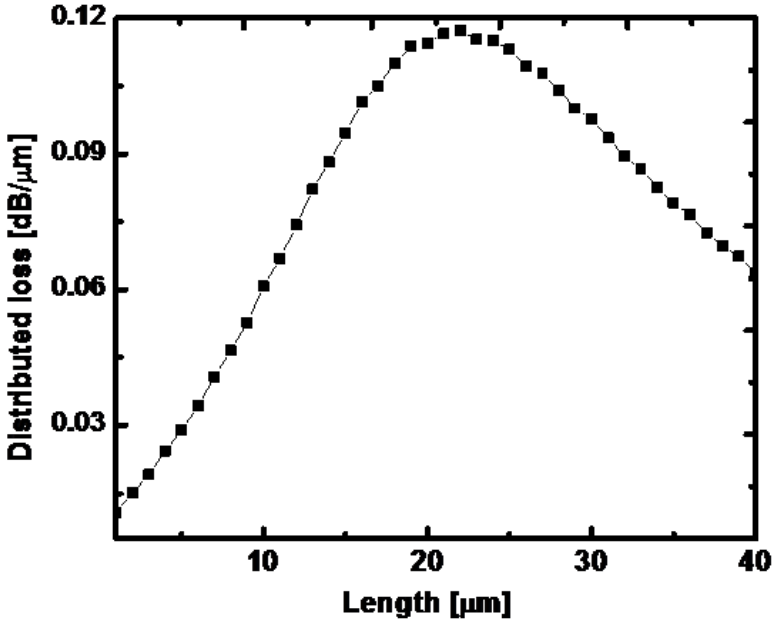

Figure 2.6: Calculated distributed loss as a function of length.

together, this structure is called 2D SSC. The referred figure is a general example for 2D SSC, the structure could have only width and height reduction and still be called 2D SSC. As can be seen in Figure 2.7, the mode size is reducing along the propagation

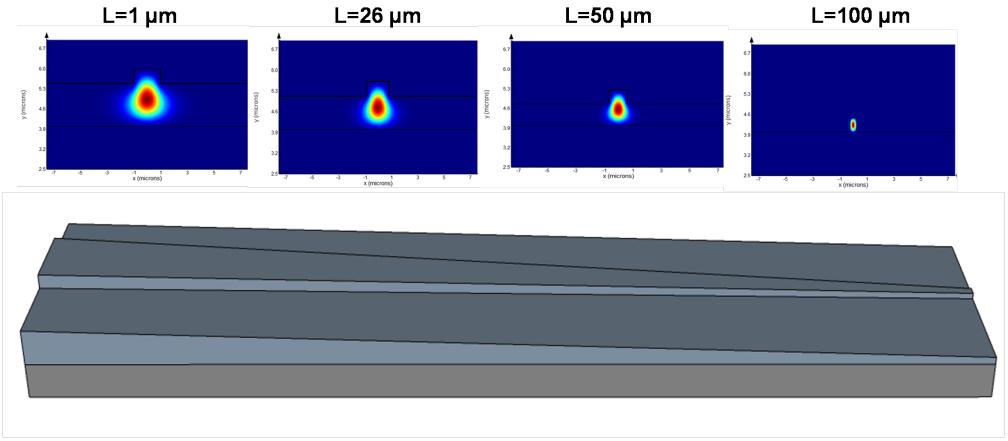

Figure 2.7: Calculated mode profiles at four different locations of 2D SSC of length 100 μm, having width variation from 2 μm to 0.5 μm, height variation from 2 μm to 0.5 μm and slab height variation from 1.5 μm to 0 μm.

direction. Figure 2.9 shows that the area is decreasing due to the cross section reduction from 4 μm^2 to 1μm^2. This SSC will enable connecting two different cross sections together in a chip. The effective modal area has been calculated with the help of following

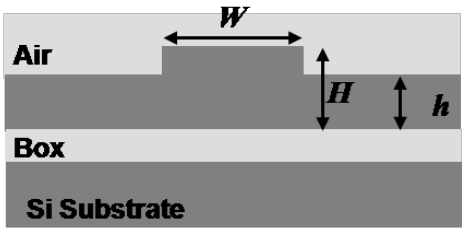

Figure 2.8: Rib waveguide cross section considered for 2D SSC.

equation :

$$A_{eff} = \frac{[\int E^2(x,y)dxdy]^2}{[\int E^4(x,y)dxdy]} \tag{2.16}$$

Here E(x,y) - Mode field distribution

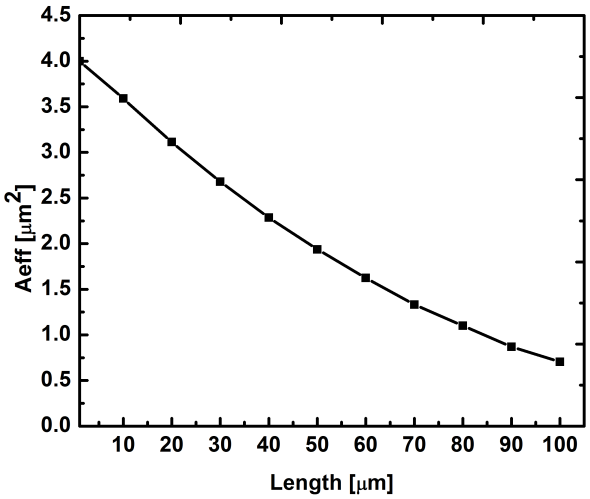

Figure 2.9: Calculated effective area A_{eff} of guided mode propagating through a 2D SSC of length 100 μm having width variation from 2 μm to 0.5 μm, height variation from 2 μm to 0.5 μm and slab height variation from 1.5 μm to 0 μm

2.3.1 Condition for single mode propagation in 2D SSC

Single mode condition for homogeneous rib waveguide is straight forward. But it is challenging in the case of SSC as the structure is considered to be stack of many waveguide cross sections kept together.

The initial larger cross section and the final smaller cross section waveguides could be designed as single mode. But it is challenging to design a whole propagation region

region of SSC to be single mode. There is a probability that when light travels from larger to smaller cross section waveguide through a tapered structure, multimode region can occur. Since the mutimode is not supported, they leak away leading to mode conversion loss while propagation.

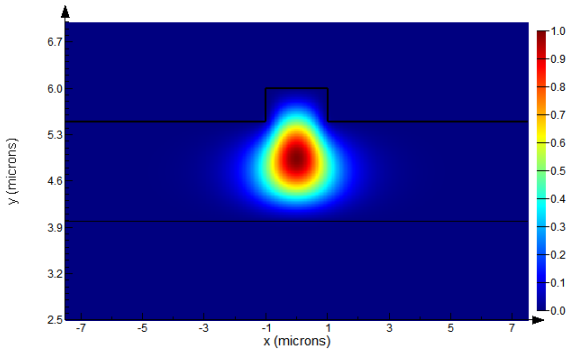

(a)

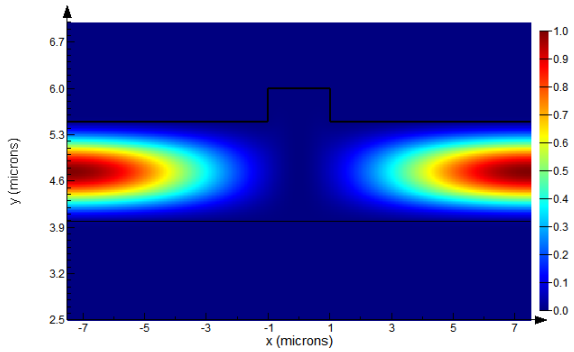

(b)

Figure 2.10: Mode profiles of TE_0 (a) and TE_1 (b) in a rib waveguide having width (W) = 2 μm, height (H) = 2 μm, slab height (h) = 1.5 μm.

The stacked structure have been solved for their mode field distribution in Lumerical MODE solver as a function of length. For understanding the multimode loss, the effective indices of fundamental mode TE_0 and first order mode TE_1 were calculated and compared with fundamental mode of slab waveguide TE_0. According to the single mode condition, fundamental mode TE_0 effective index should be higher than TE_1 and slab TE_0, which will avoid any mode conversion in the SSC. The dimensions which is chosen in this 2D SSC is single mode through out its length. The same calculation could be calculated for TM polarization for supporting single mode guidance of both the polarization.

As the cross section reduces towards end of the SSC, the mode field interaction with

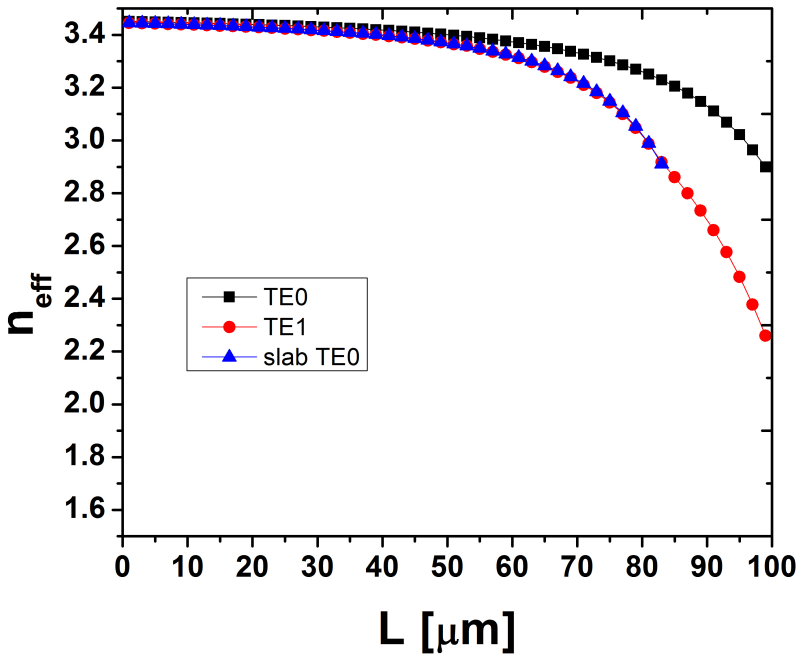

Figure 2.11: Calculated effective indices of guided TE_0, TE_1 and the slab TE_0 modes to verify single mode guidance along a SSC length 100 μm having width variation from 2 μm to 0.5 μm, height variation from 2 μm to 0.5 μm and slab height variation from 1.5 μm to 0 μm.

the sidewall increases which results in increased loss, for a given value of roughness and correlation length. The above model considers the roughness in sidewall and does not considers roughness in top surface.

2.3.2 Numerical model for calculation of scattering loss in 2D SSC

In a general SSC structure, roughness can prevail in top surface and sidewalls.The loss in the case of 2D SSC is generally a function of height, slab height and width variations with a particular cross section of the waveguide.

$$\alpha(Z) = A(S_w(Z) + S_H(Z) + S_h(Z)) \tag{2.17}$$

Where,

$$S_w(Z) = \frac{dn_{eff}}{dW}(Z) \tag{2.18}$$

$$S_H(Z) = \frac{dn_{eff}}{dH}(Z) \tag{2.19}$$

$$S_h(Z) = \frac{dn_{eff}}{dh}(Z) \tag{2.20}$$

W, H and h are width, height and slab height respectively. The term A relates to roughness and correlation length. The detailed derivation for A is given in [24].

The above equation accounts effective index change due to dimensional variations at a particular point of the waveguide. This equation could be used to model the said structure by calculating distributed parameters. The distributed parameters are dn_{eff}/dW (Z), dn_{eff}/dH (Z), dn_{eff}/dh (Z) and distributed loss α(Z) in the propagation direction of the SSC. Here Z denotes propagation direction of the waveguide. Figure 2.12 shows the effective index variation along the length. As the dimension reduces, the effective index also reduces.

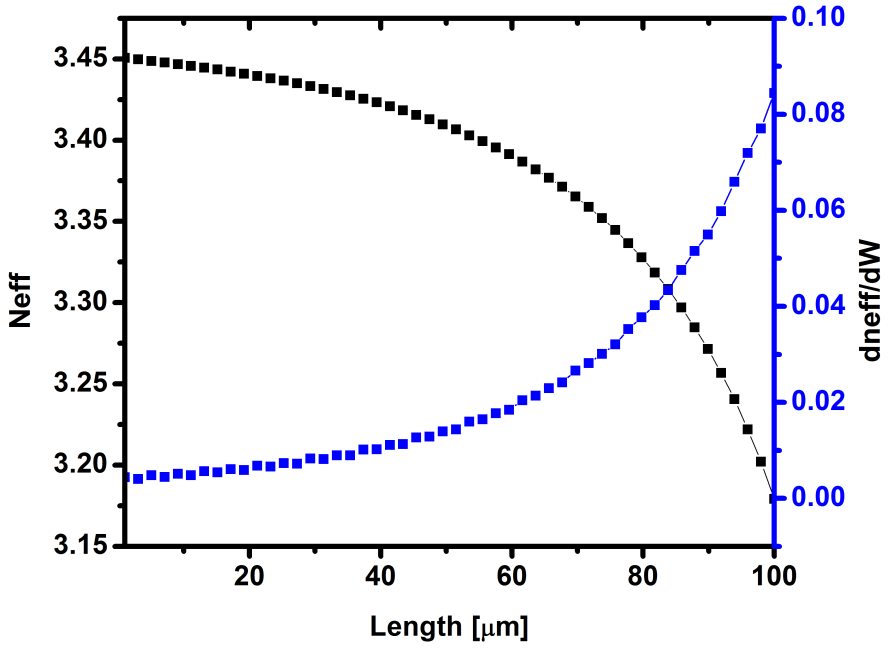

Figure 2.12: Calculated n_{eff} and dn_{eff} /dW as a function of length for a 2D SSC of length 100 μm.

In the same structure, the height, width and slab height has been changed to calculate dn_{eff}/dW (Z), dn_{eff}/dH (Z), dn_{eff}/dh (Z) respectively as shown in Figures 2.12 and 2.13. Thus the distributed loss at each point has been calculated considering the roughness at the top and sidewalls using the above equation. The variation in the total

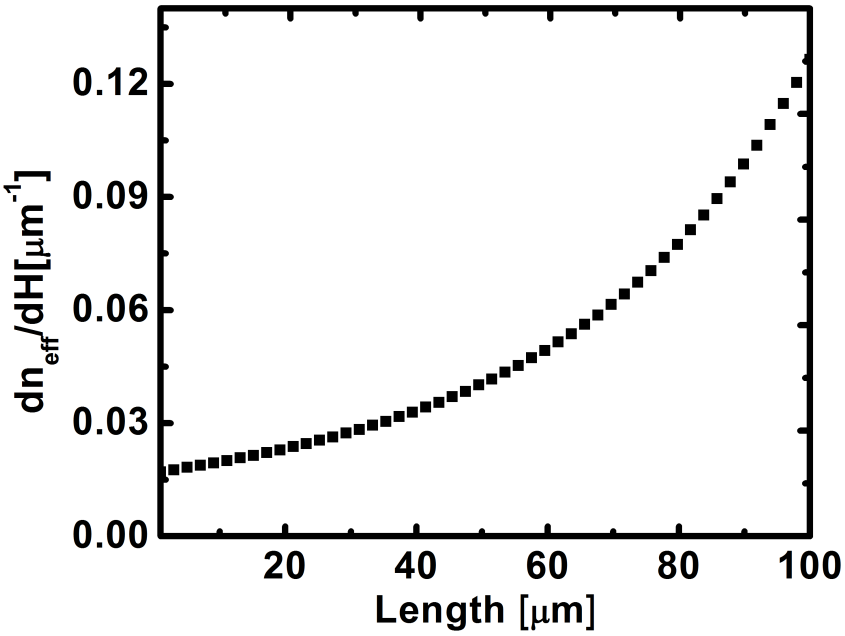

(a)

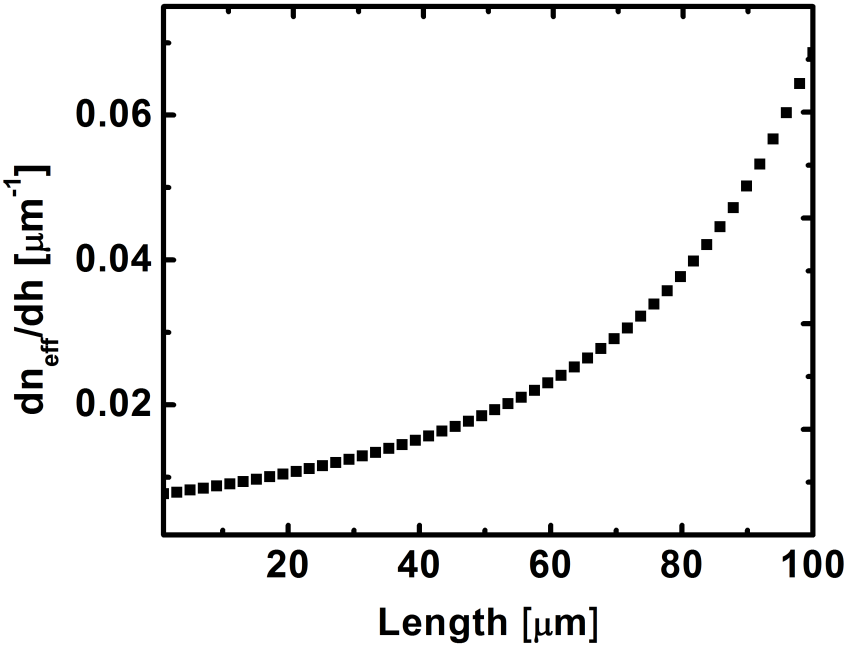

(b)

Figure 2.13: Calculated dn_{eff} /dH and dn_{eff} /dh as a function of length for a 2D SSC of length 100 μm.

height, slab height and width are defined by an equation.

$$W(Z) = W_0 - m_1 L \tag{2.21}$$

$$H(Z) = H_0 - m_2 L \tag{2.22}$$

$$h(Z) = h_0 - m_3 L \tag{2.23}$$

where, m_1, m_2, m_3 - Slopes of width, Height and slab height respectively ; L- SSC length

Later, this equation was fed to commercially available Lumerical MODE solver for effective index calculation. The mode solver will choose the defined cross section at any point of SSC length.

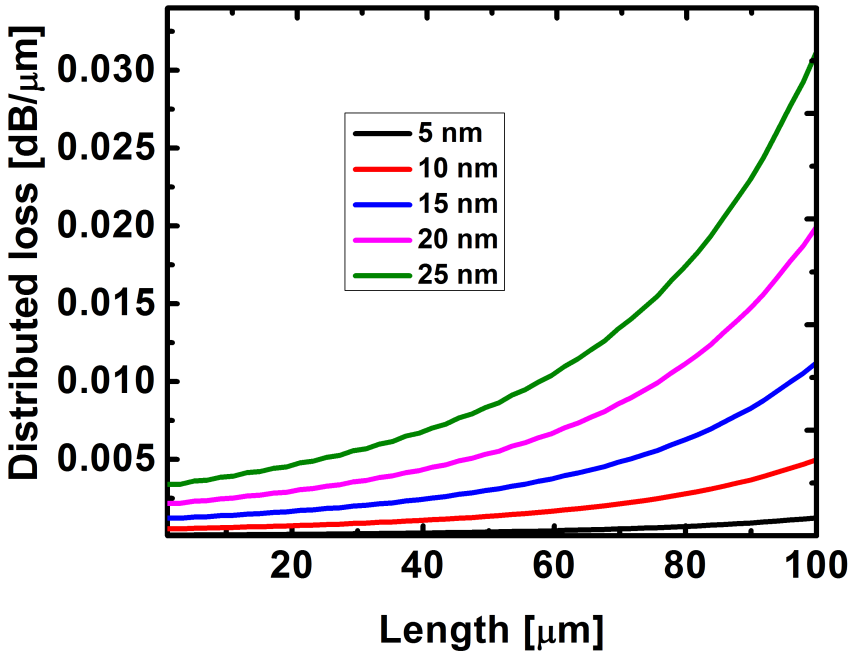

Figure 2.14: Calculated distributed loss as a function of length for varying roughness.

The RMS roughness value was taken to be 20 nm and the correlation length was kept as 60 nm and distribution loss was calculated. The RMS value of roughness determines the distributed loss in SSC. In this model, roughness and its associated correlation length (1/e width of roughness) has been considered as fitting parameters. The effect of roughness variation in distributed loss calculation is shown in Figure 2.14. The insertion loss can be calculated by taking an integration of distributed loss over the length of the SSC.

$$\alpha_T = \int_{Z=0}^{Z=L} \alpha(Z) dZ \tag{2.24}$$

By using this method, insertion loss per SSC (α_T) has been calculated to be 1.05 dB. This is due to roughness presence for a longer length. The height and slab height will have the same effect when the slope is changed. The roughness in the slab area might have lesser effect when compared to height and width of the waveguide. This is because the interaction of roughness with electric field at the slab is less compared to interfaces of side and top surface roughness interaction.

2.4 Conclusion

A generalized model has been proposed for estimating the scattering loss in 1D and 2D SSCs. The model accounts for many influential parameters of SSC design keeping the roughness and correlation length as fitting parameters as they are derived from experiments. In the described SSC the magnitude of roughness could be different in the sidewall and the top. The correlation is bound to vary following the roughness. In that case , the equation can be generalized as follows

$$\alpha(Z) = (A_1 S_w(Z) + A_2 S_H(Z) + A_3 S_h(Z)) \tag{2.25}$$

The terms A_1, A_2 and A_3 includes roughness in sidewall, surface roughness above total height and surface roughness near slab height, taking the other parameters from corresponding waveguide structure. The same model effective is in estimating loss of any SSC which is varying along propagation direction.

CHAPTER 3

Theoretical results and experimental validation

In this chapter, the model discussed in the chapter 2, has been validated with the experimentally fabricated structures. The model has been applied to inverse taper based 1D SSC and forward taper based 2D SSC. Different cross sections and SSC profiles as reported in the validating SSCs have been considered in the model.

3.1 Validation of the model with 1D SSC

In order to generalize the model for wide application, the model has been applied to inverse taper structure . The inverse taper structure has smaller cross dimension and has higher final cross dimension. Inverse tapers based on photonic wire can have slab region or some other suitable cladding materials to modify the effective index of the waveguide. The profile variation has to be accounted in the model and most of the reported inverse tapered structures have variation in width. The equation in this case, changes as below.

$$\alpha(Z) = A_1 S_w(Z); \tag{3.1}$$

$$S_w(Z) = \frac{dn_{eff}}{dW} \tag{3.2}$$

A_1 represents the component of RMS roughness and correlation length as discussed earlier. The shortfall of photonic wire based structure is that it suffers an additional loss of mode conversion loss in addition to scattering loss. Scattering loss mentioned in these reported literatures have been taken as reference to apply our model. In the literature [1], the width is varying from 120 nm to 450 nm in a parabolic function to make an adiabatic transition. Table 3.1 shows the calculated scattering loss for both these SSCs for the corresponding roughness and correlation length. In [25], effect of inverse taper

with sidewall roughness has been studied using FDTD technique. The initial width of 180 nm has been varied to 450 nm in a linear way with sidewall roughness. The length of SSC has been varied to see the effect of roughness. The higher SSC length was found to be having more scattering loss as the exposure to the roughness increased.

Table 3.1: Comparison of calculated SSC loss with reported literature

Literature	σ_{rms}	$\mathbf{L}_C$	**Scattering loss (extracted)**	**Scattering loss (calculated)**
Min et al [25].,	10 nm	50 nm	0.6 dB	0.6 dB
Almeida et al [1].,	29 nm	50 nm	4.5 dB	4.5 dB

The procedure explained in chapter 2 has been followed to calculate the scattering loss for these experimental structure. For the fitting parameters mentioned in the Table 3.1, our model matches with the reported results.

3.2 Validation with 2D SSC

The model has also been validated with the experimentally fabricated SSC structure [20] of length $\sim$ 1 mm. In this fabricated structure, the total height, slab height and width are varying, on which the equation 2.16 can be applied. The structure has been fabricated to demonstrate monolithic integration of two different cross sections in silicon platform. The loss of the tapered waveguide structure has been found from the SSC waveguide arrangement as shown in Figure 3.1. Initially, the larger waveguide section helps in coupling the light from the fiber to waveguide. Then the cross section has been reduced to smaller dimensions and interfaced with a SSC.

The fabrication parameters have been optimized in terms of single mode condition for initial and final cross sections, profile of the cross sections (i.e., rectangular/trapezoidal), length at which it remains single mode in the SSC section. In the section, fabrication of waveguide with SSC is discussed and in the second subsection, characterization of the device is discussed, followed validation of the results have been discussed.

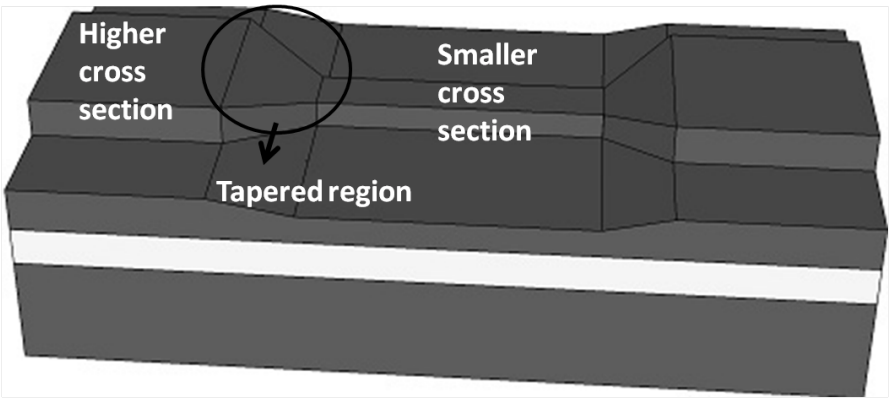

Figure 3.1: SSC integrated with two different rib waveguide cross sections.

3.3 Fabrication of forward taper based 2D SSC

In this section, the fabrication of 2D SSC structure has been discussed. This structure has been fabricated in-house to validate the model.

3.3.1 Cleaning of SOI wafer

The device was fabricated in a SOI wafer which has a device layer thickness of 2 μm. It was a <100> cut, P-type substrate having resistivity 50 Ω/cm. The samples were cleaned, following standard CMOS cleaning procedure for silicon. Initially, the organic impurities in the silicon device layer have been removed using trichloroethylene (TCE). Samples are immersed in TCE and was boiled (120$\circ$ C) in a beaker for 2-5 min. An ultrasonic agitation was given to the sample to remove the hard dust particles which had adhered to the sample. Afterwards, the samples were cleaned by immersing them in acetone with ultrasonic agitation, followed by thorough rinsing with DI water. The acetone cleaning process helps in removing the residues left by TCE cleaning. Later, the inorganic impurities were removed in the substrate using concentrated HNO_3. The samples were immersed in nitric acid and boiled till the onset of fumes. Any inorganic impurities such as Gold, Iron that had come into crystal during the crystal growth process of silicon, will get oxidized during Nitric acid cleaning. These metal impurities could be removed using nitric acid by oxidizing. Cleaning with HNO_3 not only dissolves inorganic impurities but also grows a thin oxide layer (< 5 nm) on top of silicon wafer. Metal impurities can also be removed using RCA cleaning. The growth of oxide-

film can be verified by hydrophilic nature of wafer surface. This oxide is removed by immersing the wafer in diluted HF solution (1:10 :: HF:DI water) for 30 s. The device layer becomes hydrophobic after cleaning with Hydrofluoric acid. The cleaning of the sample was ensured by inspecting them under microscope.

3.3.2 E-beam lithography

E-beam lithography was done on the cleaned SOI sample. The rationale behind choosing e-beam lithography over photolithography was to avoid pattern induced roughness, arises during photolithography. The pattern induced roughness is more detrimental in this case as there are two dry etching process.

The second dry etching process, which was a blanket etching, would increase the sidewall roughness which was already in place from the first dry etching of the waveguide. The e-beam lithography was performed in Raith 150(Two) machine. The cleaned samples are prone to acquire the moisture which may affect the uniformity of the e-beam resist coating. The sample was kept in 120$\circ$C oven to remove the moisture content. Then negative tone HSQ was spun on the sample. The spinning parameters are as follows :

1) Speed - 3000 rpm

2) Acceleration - 1500 rpm/sec

3) Time - 40 sec

The required patterns were group of 2 μm width straight waveguides. The parameters used for writing are given below :

1) Acceleration voltage : 30 KV

2) Dose : 350 μC/cm ^{2}

The samples were developed using commercial developer MF 319 for 6 minutes. Since HSQ had high etch tolerance, it was decided to use HSQ itself as mask for further etching process as the selectivity between silicon and HSQ was high for the reactive plasma.

3.4 Dry etching- I

The samples were dry etched in a Oxford plasma 100 machine using the following parameters : Pressure- 200 mTorr, SF6:Ar-20::20 sccm, forward power -150 W at room temperature. Figure 3.2 shows the scanning electron microscope images after develop-

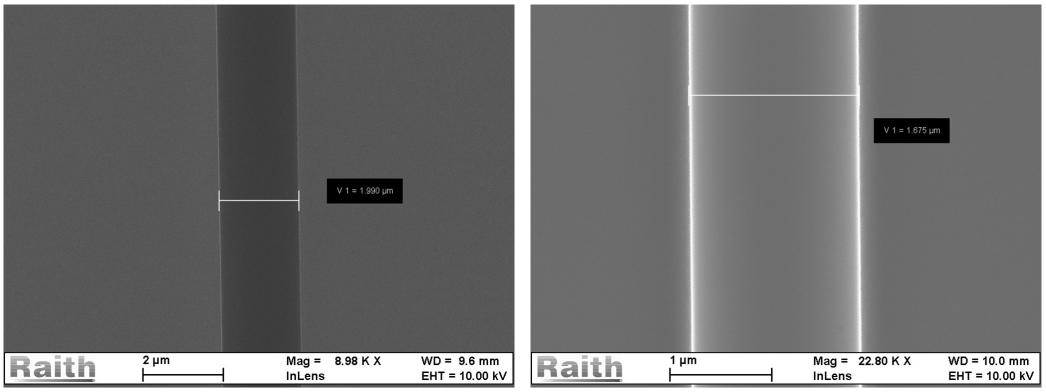

(a) (b)

Figure 3.2: (a) SEM image after e-beam lithography;(b) After first reactive ion etching.

ing the sample and after completing the fist Reactive Ion Etching (RIE). As can be seen from the images, the width of the waveguides were less than the designed value. This is due to slight over-development of HSQ and isotropic nature of the dry etching recipe. The etching depth of the waveguide was found to be 0.4 μm from confocal microscope measurement. The etch rate was optimized to be 260 nm /minute.

3.4.1 Dry etching- II

In order to get SSC structure, a shadow mask was employed after the initial experimentation. The use of shadow mask enables the plasma to go below it and etch the unexposed area as well. The structure of shadow mask has been shown in Figure 3.3. The shadow mask was a cleaned silicon wafer which was kept just above the initially fabricated straight waveguide. When etching happens, the plasma etches the exposed part and reduces the dimension proportionally and goes under shadow mask making a smooth taper section which connects a different cross sections together. The recipes used for second etching are as follows : Pressure - 250 mTorr, Flow rate - 25:25 sccm, RF power -150 W. The initial and final dimensions are given in Figures 3.4 and 3.5.

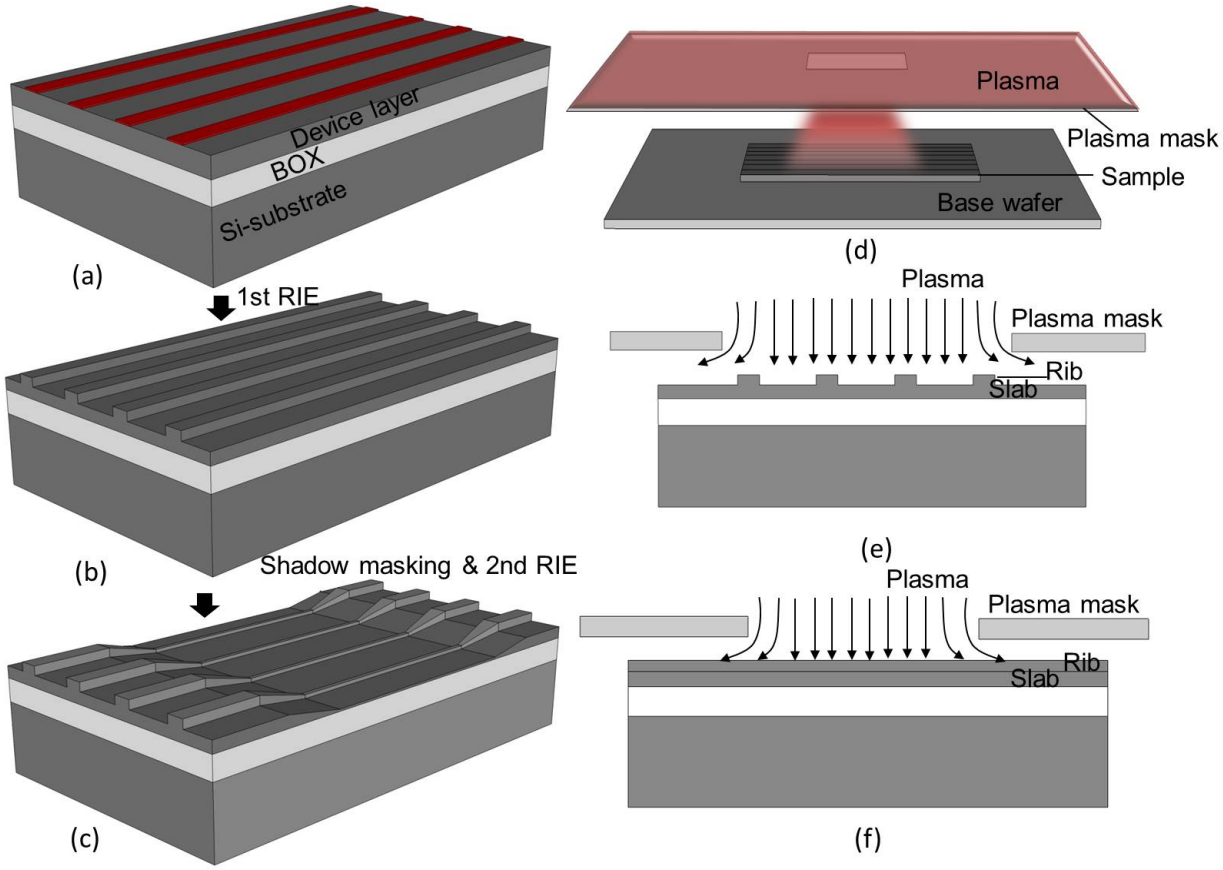

Figure 3.3: Schematic of fabrication process flow for making waveguide with SSC (a) Post E-beam Patterning; (b) After first RIE; (c) After shadow mask etching (d) Placement of shadow mask above the sample; (e),(f) Schematic of plasma residues going between the gap of Silicon sample and shadow mask.

If the structure was fabricated by photolithography process instead of a shadow mask, it would result in a step profile in the SSC section which could in turn cause increment in loss. Interestingly, the length of the SSC can be controlled by adjusting the gap between the shadow mask and the waveguide structures. The increment in length is due to presence of more plasma in the gap, in turn causes more etching. Shadow mask is nothing but a cleaned silicon sample (Standard RCA I and RCA II cleaning). The height of shadow mask is increased to observe the effect of plasma. As expected, more plasma went inside the gap in case of 1.5 mm air-gap and produced longer length.

Table 3.2: Influence of shadow mask height on taper length

Shadow mask height from substrate	SSC length
0.5 mm	1 mm
1 mm	1.5 mm
1.5 mm	2 mm

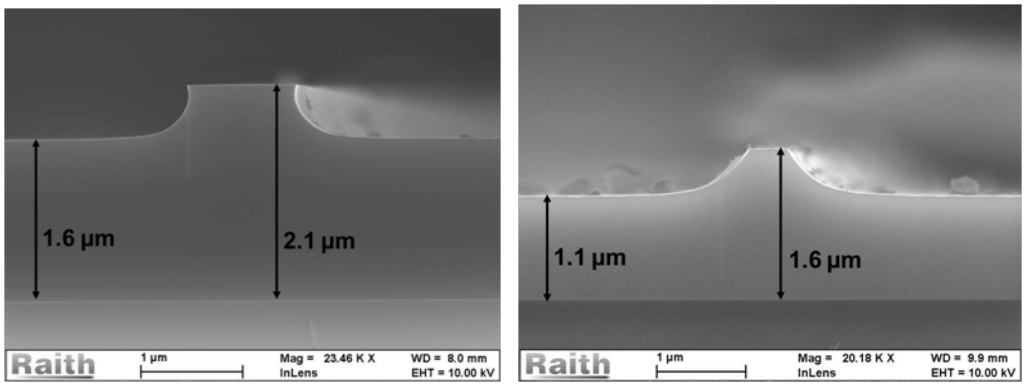

(a) (b)

Figure 3.4: SEM image of initial (a); final heights (b) of SSC.

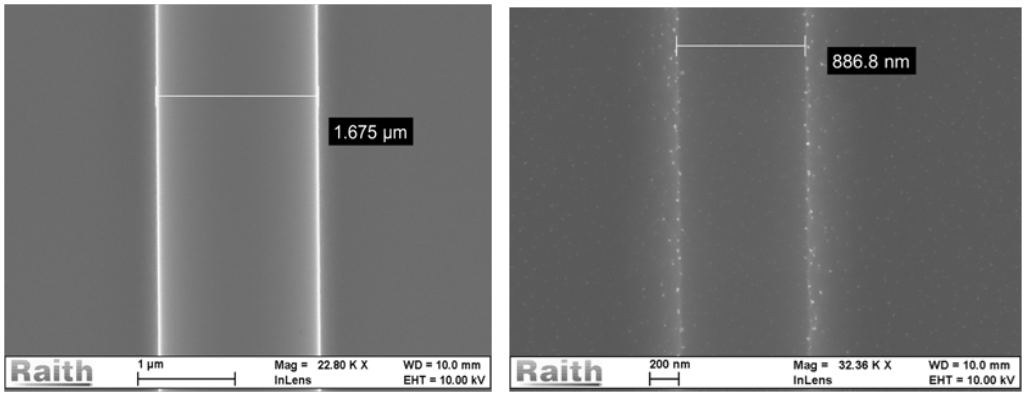

(a) (b)

Figure 3.5: SEM image of initial (a); final widths (b) of the SSC.

The end facet preparation was performed after second etching process. The SOI samples were diced to remove the rough edges in the sample. This was followed by polishing of end facet using diamond lapping films (polishing sheets) whose roughness varying from 2 μm to 100 nm. The polished samples were imaged in the microscope as shown in Figure 3.6. The image clearly shows the cross section of rib waveguide. The reference straight waveguide is denoted as untrimmed waveguide and the waveguide with SSC is denoted as trimmed waveguide.

3.4.2 Optical Characterization

The optical characterization of the sample were done in a tapered fiber coupling setup which is shown in figure 3.7. The tapered fiber was used to reduce the mode mismatch

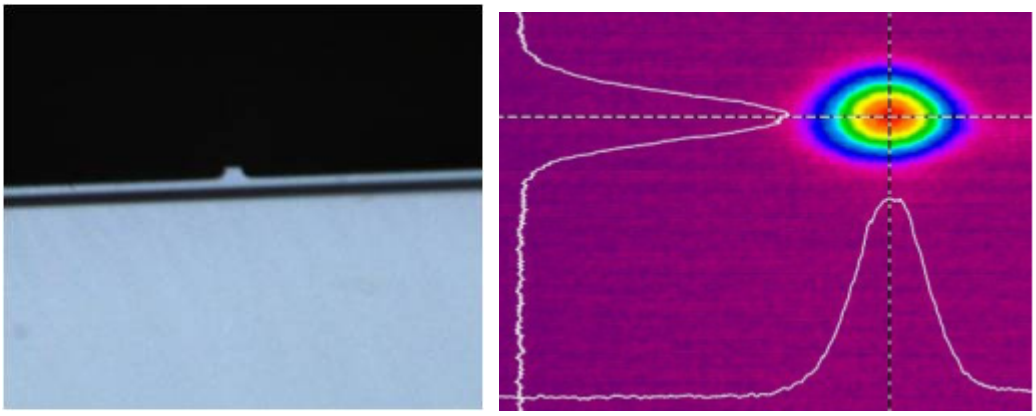

(a) (b)

Figure 3.6: (a) Polished end facet of the waveguide; (b) Measured intensity distribution of the guided mode at the larger cross section side of SSC.

loss between waveguide and fiber. The setup consists of a tunable laser source (1520 nm -1560 nm, 10 mW maximum power) connected through a polarizaiton controller to the sample. The polarization controller helps to maximize the power of particular polarization by applying the stress in the fiber.

In the output side of the sample 60X lens was used to collect the light which is coming out of the sample. The collected light is made to fall on the detector through a polarizer. The optical characterization of the sample has been done for TE polarization.

Since the end facets of the waveguides were polished well, they act like a mirror and form a cavity. This Fabry-Perot cavity is used to measure the propagation loss in the waveguide. There are two set of waveguides which are considered, i.e., untrimmed waveguide and trimmed waveguide. The trimmed waveguide structure has two different cross sections which is connected by SSCs. The untrimmed cross sections has only one cross section through out the propagation direction. This is done to understand the loss introduced due to trimming process. The Fabry Perot response of the waveguide with SSC is shown in below Figure 3.8. As can be noted from the figure that the difference between peak and the low in the Fabry-Perot spectrum is less even after incorporating the SSC with the waveguide. This means that the cavity is not much affected due to the trimming process. This shadow mask process is simple and cost effective compared to double patterning technique and gray scale lithography. The results from the optical characterization of the SSC shows that there is no induction of multimode due to the

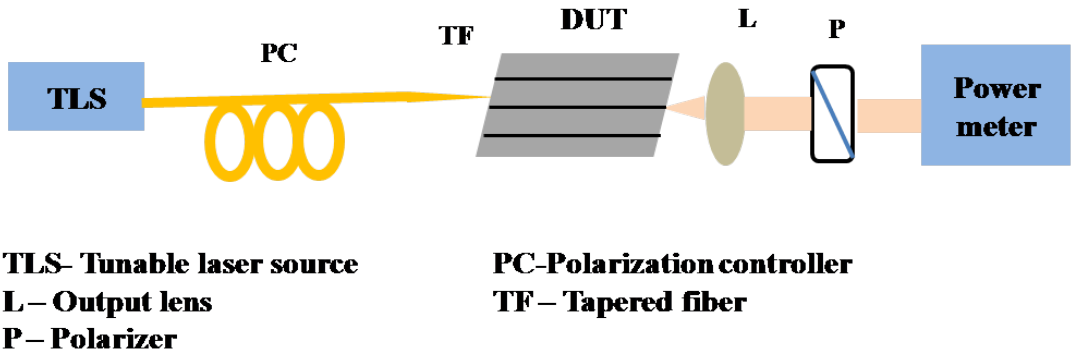

(a)

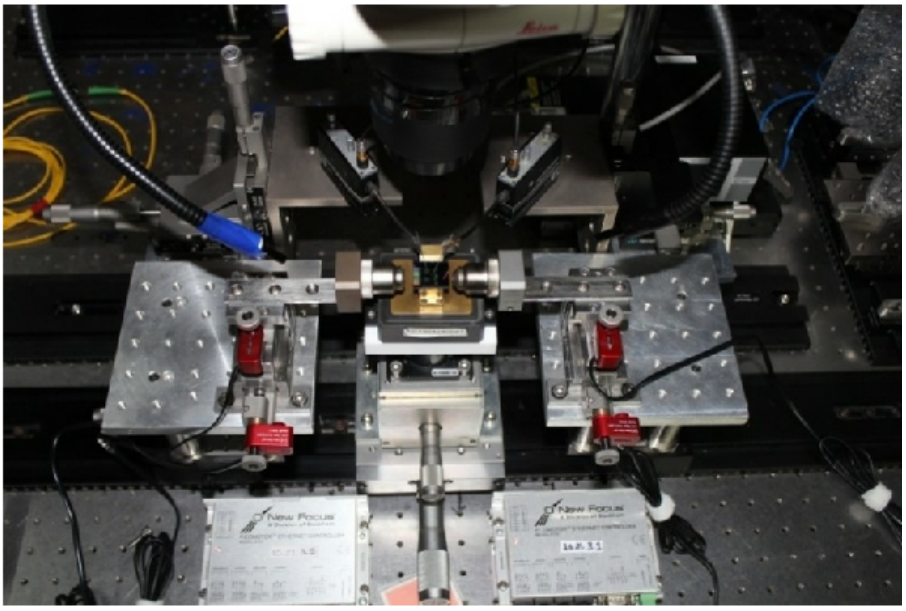

(b)

Figure 3.7: (a) Schematic of the optical characterization setup used for characterizing 2D SSC; (b) Experimental optical characterization setup.

presence of SSC. The SSC insertion loss have been calculated to be 0.25 dB (@ λ -1550 nm, TE polarization) by comparing the propagation loss of reference straight waveguide.

The dimension of the tapered SSC section have been extracted from the fabricated structure, with the help of confocal microscope and SEM. The corresponding variation of the height and width of SSC region is shown in Figures 3.9 and 3.10.

In both width and etch depth variations, initially the variation is sharp because of the placement of shadow mask between higher and lower cross section waveguide. In the second configuration, the tapering of SSC is adiabatic and gradual. The length of

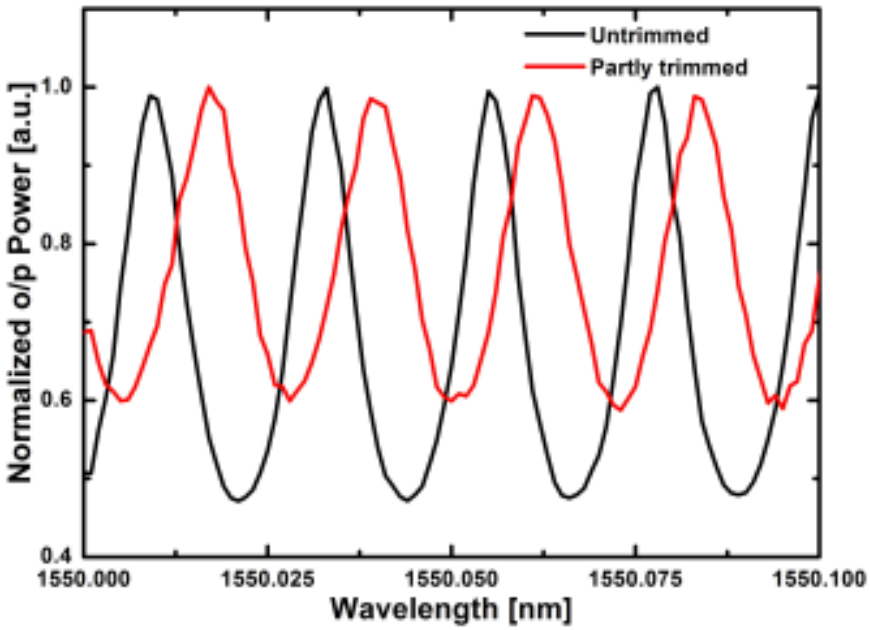

Figure 3.8: Fabry-Perot response from the reference straight waveguide (Untrimmed) and the waveguide with SSC (Trimmed)

the SSC was found to be $\sim$1 mm. The top view of SSC has been shown in Figure 3.11 (a) and the schematic of the cross section used in the calculation for modelling has been shown in Figure 3.11 (b). Because of the plasma residues used, the cross section doesn't have ideal rectangular sidewall, it becomes a trapezoidal structure, having different bottom and top width. An average of these two widths has been used for the calculation.

The extracted parameters were made to fit with the equation to understand the variation along taper length. The parameters were interpolated to get the maximum points and fitted with the equation. The extracted parameters were given as input in the proposed model to estimate the insertion loss of the SSC alone. The width and height variations have been fitted with an equation. This equation was given to Lumerical MODE solver to change the dimension with respect to length.

The SSC area follows the fit equation (explained in Appendix C), changes the cross section at each point iteratively. Thus a three dimensional problem have been broken down to two dimensional problem. It is computationally expensive to solve such a structure, which has trapezoidal cross section, roughness on sidewalls and top surface in an adiabatic variation, using commercially available FDTD electromagnetic propa-

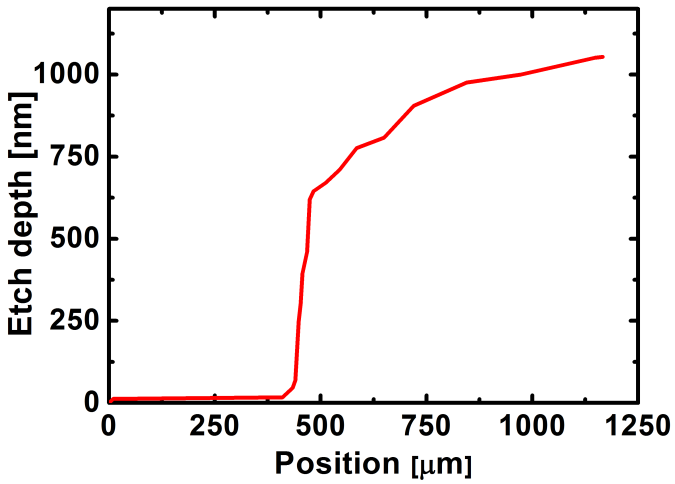

Figure 3.9: Waveguide width along SSC length

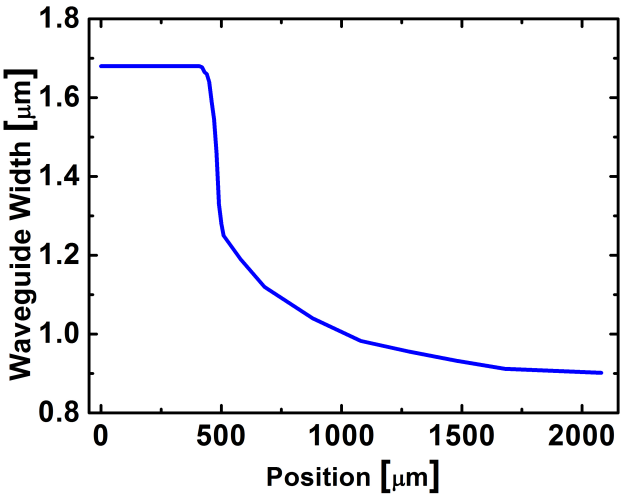

Figure 3.10: Waveguide etch depth along SSC length

gation solvers. The distributed loss for this experimetnal SSC has been shown in Figure 3.12.

3.4.3 Insertion loss calculation

The insertion loss was calculated to be 0.3 dB (for σ = 5 nm, Lc = 50 nm) from the model in a similar procedure explained for 1D SSC but the experimental value is 0.25 dB. The deviation may be attributed to choosing the right value of correlation length, effect of slab surface roughness on the propagating mode.

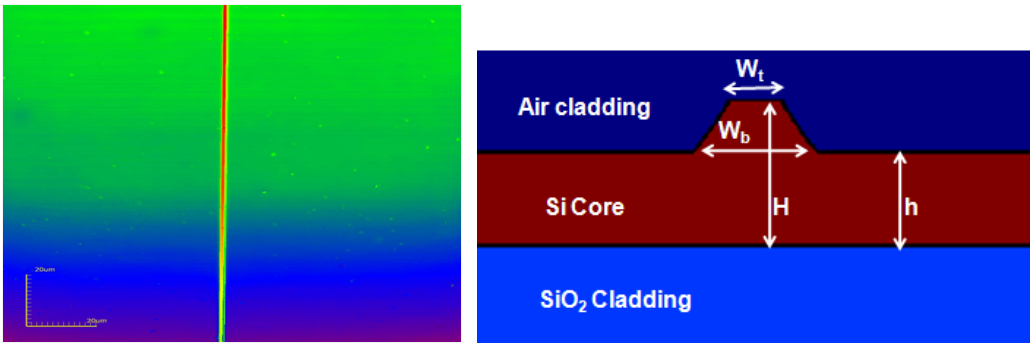

(a) (b)

Figure 3.11: (a) Top view of the fabricated 2D SSC; (b) Schematic of experimental rib waveguide cross section.

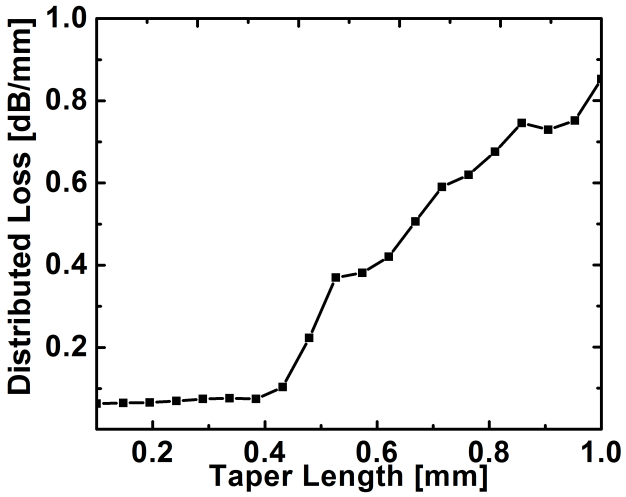

Figure 3.12: Distributed loss profile along SSC length

3.4.4 Results and Discussion

The roughness at the slab region may not contribute much to the propagation loss if the mode is well confined. The top surface roughness is also small because the sidewall component is higher. The loss was calculated to be 0.3 dB for a roughness of 5 nm, correlation length of 50 nm and the experimental loss was 0.25 dB. The mode conversion loss has not been considered as a loss component in total loss because the optical characterization results shows that the propagation loss is only due to scattering.

3.5 Conclusion

The model has been applied to reported inverse taper based 1D SSCs having linear and parabolic profiles and found to be in agreement with the scattering loss reported. The loss modeling of a experimentally fabricated 2D SSC has been discussed. The calculated loss using our model is in match with the experimental loss by the use of fitting parameters, RMS roughness and correlation length. The model has been generalized to estimate the scattering loss of any cross section, profile, length, roughness at sidewall, surface for estimating the scattering loss.

CHAPTER 4

Conclusions

4.1 Summary

A generalized model has been developed to estimate the roughness induced loss in 1D and 2D tapered SSC structures. The loss model accounts for parameters such as cross section, length, roughness in sidewall/surface and the profile of SSC variation. The same model has been applied to inverse taper based SSC structures and validated for different SSC profiles. The proposed model has also been validated with experimentally fabricated rib waveguide based adiabatic SSC structure , having a length of 1 mm. The proposed model is a novel solution for such SSCs having a long length which are mainly used for adiabatic propagation. The exact profile of the SSC have been mapped experimentally and fed to the simulation for estimating the scattering loss. The estimation involved finding out the distributed loss, later integrated the distributed loss to calculate the insertion of loss/SSC. The model considered the roughness in the sidewall, surface and the slab region. The model also accounted for trapezoidal cross section of rib waveguide which arose out of isotropic nature of the dry etching recipe used. The estimated loss of 0.3 dB using the model has been in agreement with the measured scattering loss of 0.25 dB.

The accuracy of the model is governed by the extracted parameters from the fabricated structure and fitting equations used for defining the SSC. The model considers the value of roughness and correlation length as fitting parameters as they are limited by the process recipe used for estimating the loss.

4.2 Future scopes

The applicability of the model for calculating the intensity required to realize any non-linear optical effect has been discussed in this section.

4.2.1 Intensity enhancement for nonlinear optical effects

The fabrication of the 2D SSC lead to the cross section reduction. The fabricated SSC has profound applications in realizing nonlinear optical processes. The main bottleneck of realizing nonlinear optical effect is required amount of intensity coupled from fiber to nano dimension waveguides. The intensity increment in the lower cross section, when two cross sections are integrated together through a SSCr, is an interesting phenomena to study.

Intensity enhancement at lower cross section waveguide helps to realize nonlinear optical effects such as Four Wave Mixing (FWM), Third Harmonic Generation, Stimulated Raman Scattering (SRS) etc. in silicon. While realizing any nonlinear effect, there is an effect called Two Photon Absorption (TPA), which comes to play and reduces the total intensity inside the waveguide. This non-linear loss along with linear loss which is scattering loss quantified with our proposed model, will be helpful in calculating the amount of effective intensity required to see any non-linear effect in a waveguide with SSC.

APPENDIX A

Loss estimation flow chart and algorithm

A.1 Flow chart

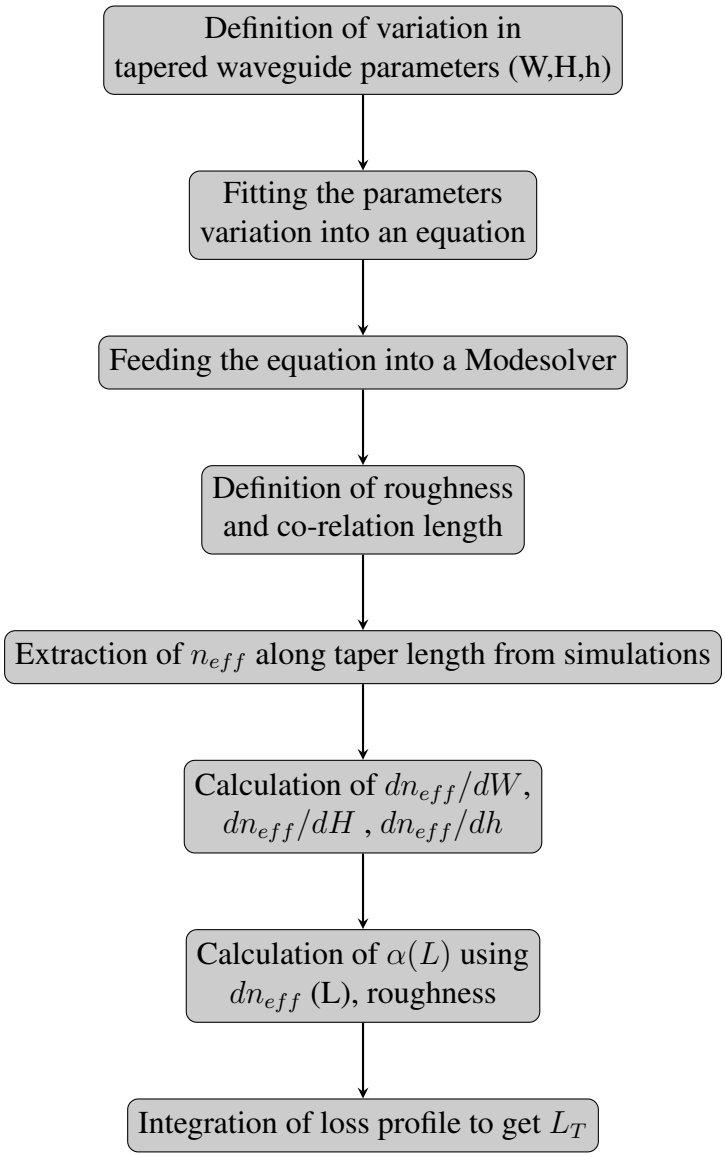

Figure A.1: Flow diagram describing the methodology of loss estimation in a tapered waveguide

APPENDIX B

Fabrication parameters

B.1 RCA-1 and RCA-2 cleaning

RCA-1 is a solution of DI water, aqueous ammonium hydroxide and aqueous hydrogen peroxide in the ratio 5:1:1. Silicon sample is boiled in this solution for about 15 minutes at 80 ° C. This removes organic residues and metallic contaminants and also forms thin layer of silicon dioxide.

RCA-2 is a solution of DI water, aqueous hydrochloric acid and aqueous hydrogen peroxide in the ratio 6:1:1. Silicon sample is boiled in this solution for about 15 minutes at 80 ° C. This removes residual metallic contaminants which were not removed by RCA-1 cleaning and also forms thin layer of silicon dioxide.

In between RCA-1 and RCA-2 clean, an oxide etching step is performed with mixture of hydrofluoric acid and DI water (1:100) and sample is rinsed in DI water and dried using compressed nitrogen.

B.2 PPR Ashing

This recipe is used to remove the residual PPR o top of wafer,, which could not be removed using acetone.
O_2 : 35 sccm
Chamber Pressure : 250 mTorr
RF Power : 150 W

APPENDIX C

Fitting parameters

C.1 Procedure for fitting

1. Experimental values of Width, height and slab height have been collected from Confocal microscope.

2. They have been interpolated using cubic spline interpolation tool in MATALB to increase the number of points.

3. The curve fitting module in MATLAB have been used to fit the above equation with the multiple sine wave function.

4. The goodness of fit have been found to be 97

C.1.1 Fit parameters for Width, Height and Slab height

The experimental width parameter was fit into an multi-sine equation and the co-efficients of the equations are mentioned below:

W1 =(a1*sin(b1*L+c1) + a2*sin(b2*L+c2) +a3*sin(b3*L+c3) + a4*sin(b4*L+c4) + a5*sin(b5*L+c5) + a6*sin(b6*L+c6) + a7*sin(b7*L+c7) + a8*sin(b8*L+c8))

a1 = 1.661e-06 ;

b1 = 1571 ;

c1 = 0.2102 ;

a2 = 9.479e-07 ;

b2 = 3142 ;

c2 = 1.611 ;

a3 = 1.601e-07 ;

b3 = 6283 ;

c3 = 1.132 ;

a4 = 4.899e-08 ;

b4 = 1.571e+04 ;

c4 = 1.69 ;

a5 = 4.792e-08 ;

b5 = 1.257e+04 ;

c5 = 2.402 ;

a6 = 2.904e-08 ;

b6 = 1.885e+04 ;

c6 = 0.8565 ;

a7 = 2.129e-08 ;

b7 = 9425 ;

c7 = 1.624 ;

a8 = 1.878e-08 ;

b8 = 2.827e+04 ;

c8 = 1.96 ;

The total reduction of a height in the experimentally fabricated has been fit into an equation as below,

H1 = H-((a11*sin(b11*L+c11) + a12*sin(b12*L+c12) +
a13*sin(b13*L+c13) + a14*sin(b14*L+c14) +
a15*sin(b15*L+c15) + a16*sin(b16*L+c16) +
a17*sin(b17*L+c17) + a18*sin(b18*L+c18)))

a11 = 1.034e-06 ;

b11 = 2618 ;

c11 = -0.5173 ;

a12 = 3.054e-07 ;

b12 = 5236 ;

c12 = 1.974 ;

a13 = 1.758e-07 ;

b13 = 1.047e+04 ;

c13 = 1.347 ;

a14 = 5.563e-08 ;

b14 = 2.094e+04 ;

c14 = 2.652 ;

a15 = 4.325e-08 ;

b15 = 2.618e+04 ;

c15 = 0.7822 ;

a16 = 2.682e-08 ;

b16 = 3.665e+04 ;

c16 = 2.019 ;

a17 = 3.628e-08 ;

b17 = 1.571e+04 ;

c17 = -0.3501 ;

a18 = 2.08e-08 ;

b18 = 3.142e+04 ;

c18 = -2.021 ;

The total reduction of a slab height in the experimentally fabricated has been fit into an equation as below,

h1=h0-((a111*sin(b111*L+c111) + a211*sin(b211*L+c211) + a311*sin(b311*L+c311) + a411*sin(b411*L+c411) + a511*sin(b511*L+c511) + a611*sin(b611*L+c611) + a711*sin(b711*L+ + a811*sin(b811*L+c811)))

a111 = 8.662e-07;

b111 = 2697;

c111 = -0.4807 ;

a211 = 2.542e-07;

b211 = 5393;

c211= 1.89 ;

a311 = 1.201e-07;

b311 = 1.079e+04;

c311 = 1.485;

a411 = 3.955e-08;

b411 = 2.157e+04;

c411 = 2.426;

a511 = 2.2e-08;

b511 = 2.697e+04;

c511 = 0.8722;

a611 = 1.961e-08;

b611 = 3.775e+04;

c611 = 1.848 ;

a711 = 1.494e-08;

b711 = 3.236e+04;

c711 = -2.695;

a811 = 1.335e-08;

b811 = 4.854e+04;

c811 = 2.869;

REFERENCES

[1] V. R. Almeida, R. R. Panepucci, and M. Lipson, "Nanotaper for compact mode conversion," *Optics Letters*, vol. 28, no. 15, pp. 1302–1304, 2003.

[2] R. Liu, Y. Wang, D. Yin, H. Ye, X. Yang, and Q. Han, "A high-efficiency grating coupler between single-mode fiber and silicon-on-insulator waveguide," *Journal of Semiconductors*, vol. 38, no. 5, p. 054007, 2017.

[3] Y. Xiong, D.-X. Xu, J. H. Schmid, P. Cheben, S. Janz, and W. Ye, "Robust silicon waveguide polarization rotator with an amorphous silicon overlayer," *IEEE Photon. J.*, vol. 6, no. 2, p. 2200308, 2014.

[4] C. T. DeRose, M. Watts, R. W. Young, D. C. Trotter, G. N. Nielson, W. Zortman, and R. D. Kekatpure, "Low power and broadband 2 x 2 silicon thermo-optic switch," in *Optical Fiber Communication Conference*. Optical Society of America, 2011, p. OThM3.

[5] D. Thomson, A. Zilkie, J. E. Bowers, T. Komljenovic, G. T. Reed, L. Vivien, D. Marris-Morini, E. Cassan, L. Virot, J.-M. Fédéli *et al.*, "Roadmap on silicon photonics," *Journal of Optics*, vol. 18, no. 7, p. 073003, 2016.

[6] T. Claes, J. G. Molera, K. De Vos, E. Schacht, R. Baets, and P. Bienstman, "Label-free biosensing with a slot-waveguide-based ring resonator in silicon on insulator," *IEEE Photonics journal*, vol. 1, no. 3, pp. 197–204, 2009.

[7] D. Bonneau, J. W. Silverstone, and M. G. Thompson, "Silicon quantum photonics," in *Silicon Photonics III*. Springer, 2016, pp. 41–82.

[8] R. A. Soref, "Silicon-based optoelectronics," *Proceedings of the IEEE*, vol. 81, no. 12, pp. 1687–1706, 1993.

[9] W. Bogaerts, "Nanophotonic waveguides and photonic crystals in silicon-on-insulator." 2002.

[10] A. Densmore, D.-X. Xu, S. Janz, P. Waldron, J. Lapointe, T. Mischki, G. Lopinski, A. Delâge, J. Schmid, and P. Cheben, "Sensitive label-free biomolecular detection using thin silicon waveguides," *Advances in optical technologies*, vol. 2008, 2008.

[11] A. Khilo, M. A. Popović, M. Araghchini, and F. X. Kärtner, "Efficient planar fiber-to-chip coupler based on two-stage adiabatic evolution," *Optics express*, vol. 18, no. 15, pp. 15 790–15 806, 2010.

[12] J. Schrauwen, D. Van Thourhout, and R. Baets, "Trimming of silicon ring resonator by electron beam induced compaction and strain," *Optics Express*, vol. 16, no. 6, pp. 3738–3743, 2008.

[13] L. Zhou, K. Okamoto, and S. Yoo, "Athermalizing and trimming of slotted silicon microring resonators with uv-sensitive pmma upper-cladding," *Photonics Technology Letters, IEEE*, vol. 21, no. 17, pp. 1175–1177, 2009.

[14] A. Canciamilla, F. Morichetti, S. Grillanda, P. Velha, M. Sorel, V. Singh, A. Agarwal, L. C. Kimerling, and A. Melloni, "Photo-induced trimming of chalcogenide-assisted silicon waveguides," *Optics Express*, vol. 20, no. 14, pp. 15 807–15 817, 2012.

[15] S. Grillanda, V. Raghunathan, V. Singh, F. Morichetti, J. Michel, L. Kimerling, A. Melloni, and A. Agarwal, "Post-fabrication trimming of athermal silicon waveguides," *Optics Letters*, vol. 38, no. 24, pp. 5450–5453, 2013.

[16] T. Lipka, M. Kiepsch, H. K. Trieu, and J. Müller, "Hydrogenated amorphous silicon photonic device trimming by uv-irradiation," *Optics express*, vol. 22, no. 10, pp. 12 122–12 132, 2014.

[17] S. Chandran, M. Sundaram, S. Kurudi, and B. K. Das, "Design and fabrication of surface trimmed silicon-on-insulator waveguide with adiabatic spot-size converters," *Applied Optics*, vol. 56, no. 6, pp. 1708–1716, 2017.

[18] R. Takei, M. Suzuki, E. Omoda, S. Manako, T. Kamei, M. Mori, and Y. Sakakibara, "Silicon knife-edge taper waveguide for ultralow-loss spot-size converter fabricated by photolithography," *Applied Physics Letters*, vol. 102, no. 10, p. 101108, 2013.

[19] N.-N. Feng, S. Liao, D. Feng, X. Wang, P. Dong, H. Liang, C.-C. Kung, W. Qian, Y. Liu, J. Fong *et al.*, "Design and fabrication of 3μm silicon-on-insulator waveguide integrated ge electro-absorption modulator," *Optics express*, vol. 19, no. 9, pp. 8715–8720, 2011.

[20] S. Chandran and B. K. Das, "Tapering and size reduction of single-mode silicon waveguides by maskless rie," in *Opto-Electronics and Communications Conference (OECC), 2012 17th*, July 2012, pp. 655–656.

[21] Q. Xia, P. F. Murphy, H. Gao, and S. Y. Chou, "Ultrafast and selective reduction of sidewall roughness in silicon waveguides using self-perfection by liquefaction," *Nanotechnology*, vol. 20, no. 34, p. 345302, 2009.

[22] J. Lacey and F. Payne, "Radiation loss from planar waveguides with random wall imperfections," *IEE Proceedings J-Optoelectronics*, vol. 137, no. 4, pp. 282–288, 1990.

[23] E. Jaberansary, T. M. B. Masaud, M. Milosevic, M. Nedeljkovic, G. Z. Mashanovich, and H. M. Chong, "Scattering loss estimation using 2-d fourier analysis and modeling of sidewall roughness on optical waveguides," *IEEE Photonics Journal*, vol. 5, no. 3, pp. 6 601 010–6 601 010, 2013.

[24] D. Melati, F. Morichetti, and A. Melloni, "A unified approach for radiative losses and backscattering in optical waveguides," *Journal of Optics*, vol. 16, no. 5, p. 055502, 2014. [Online]. Available: http://stacks.iop.org/2040-8986/16/i=5/a=055502

[25] T. Min, B. Niu, K. Han, and M. Qi, “Effect of waveguide surface roughness on the fiber coupling efficiency of inverse tapers,” in *Optical Fiber Communication Conference*. Optical Society of America, 2015, pp. Th3F–6.

LIST OF PUBLICATIONS

Journal

1. Sujith Chandran, Meenatchi Sundaram, Sreevatsa Kurudi, and Bijoy Krishna Das, "Design and fabrication of surface trimmed silicon-on-insulator waveguide with adiabatic spot-size converters," Appl. Opt. 56, 1708-1716 (2017).

Patent

1. S. Chandran, S. M. Sundaram and B. K. Das, Method and apparatus for modifying dimensions of a waveguide, Filing reference for Indian patent - 3799/CHE/2015 and for US Patent - 15/218,300.

Conference

1. S.M. Sundaram, S. Chandran and B.K. Das, "Loss Estimation of Adiabatically Tapered Silicon Waveguides", Oral Presentation, ICAOP-2017 (41st OSI), Hisar, India (23-26 November 2017)